

1       **Global Meteorological Drought: A Synthesis of Current Understanding with a**  
2                                   **Focus on SST Drivers of Precipitation Deficits**

3  
4     S. Schubert\*<sup>1</sup>, R. Stewart<sup>2</sup>, H. Wang<sup>1,3</sup>, M. Barlow<sup>4</sup>, H. Berbery<sup>5</sup>, W. Cai<sup>6</sup>, M. Hoerling<sup>7</sup>,  
5     K. Kanikicharla<sup>8</sup>, R. Koster<sup>1</sup>, B. Lyon<sup>9</sup>, A. Mariotti<sup>10</sup>, C. R. Mechoso<sup>11</sup>, O. Müller<sup>12</sup>, B.  
6             Rodriguez-Fonseca<sup>13</sup>, R. Seager<sup>14</sup>, S.I. Seneviratne<sup>15</sup>, L. Zhang<sup>16</sup>, T. Zhou<sup>16</sup>

7  
8     <sup>1</sup>*Global Modeling and Assimilation Office, NASA GSFC, Greenbelt, MD, USA*

9     <sup>2</sup>*University of Manitoba, Department of Environment and Geography, Winnipeg, Canada*

10    <sup>3</sup>*Science Systems and Applications, Inc., Lanham, MD, USA*

11    <sup>4</sup>*University of Massachusetts Lowell, Lowell, MA, USA*

12    <sup>5</sup>*Earth System Science Interdisciplinary Center/Cooperative Institute for Climate and*  
13    <sup>5</sup>*Satellites, University of MD, College Park, MD, USA*

14    <sup>6</sup>*CSIRO Marine and Atmospheric Research, Aspendale, Victoria, Australia*

15    <sup>7</sup>*NOAA Earth System Research Laboratory, Boulder, CO, USA*

16    <sup>8</sup>*Indian Institute of Tropical Meteorology, Pune, India*

17    <sup>9</sup>*International Research Institute for Climate and Society, The Earth Institute, Columbia*  
18    <sup>9</sup>*University, Palisades, NY, USA*

19    <sup>10</sup>*NOAA/OAR Climate Program Office, Silver Spring, MD, USA*

20    <sup>11</sup>*Department of Atmospheric and Oceanic Sciences, University of California, Los*  
21    <sup>11</sup>*Angeles, CA, USA*

22    <sup>12</sup>*CEVARCAM, Facultad de Ingeniería y Ciencias Hídricas 5, Universidad Nacional del*  
23    <sup>12</sup>*Litoral and CONICET, Santa Fe, Argentina*

24    <sup>13</sup>*Departamento de Física de la Tierra, Astronomía y Astrofísica-I, Facultad de CC.*  
25    <sup>13</sup>*Físicas, Madrid, Spain.*

26    <sup>14</sup>*Lamont Doherty Earth Observatory of Columbia University, Palisades, NY, USA*

27    <sup>15</sup>*Institute for Atmospheric and Climate Science, ETH, Zürich, Switzerland*

28    <sup>16</sup>*LASG, Institute of Atmospheric Physics, Chinese Academy of Sciences, Beijing, China*  
29

30                                   Revision Submitted to

31                                   Journal of Climate GDIS Special Collection

32                                   19 January 2016

33     \*Corresponding author address: Siegfried Schubert, 8800 Greenbelt Rd.,  
34     NASA/GSFC, Greenbelt, MD 20771. E-mail: [siegfried.d.schubert@nasa.gov](mailto:siegfried.d.schubert@nasa.gov)

35 ABSTRACT

36

37 Drought affects virtually every region of the world, and potential shifts in its character in  
38 a changing climate are a major concern. This article presents a synthesis of current  
39 understanding of meteorological drought, with a focus on the large-scale controls on  
40 precipitation afforded by sea surface temperature (SST anomalies), land surface  
41 feedbacks, and radiative forcings. The synthesis is primarily based on regionally-focused  
42 articles submitted to the Global Drought Information System (GDIS) collection together  
43 with new results from a suite of atmospheric general circulation model experiments  
44 intended to integrate those studies into a coherent view of drought worldwide. On  
45 interannual time scales, the preeminence of ENSO as a driver of meteorological drought  
46 throughout much of the Americas, eastern Asia, Australia and the Maritime Continent is  
47 now well established, whereas in other regions (e.g., Europe, Africa and India), the  
48 response to ENSO is more ephemeral or non-existent. Northern Eurasia, central Europe  
49 as well as central and eastern Canada stand out as regions with little SST-forced impacts  
50 on precipitation on interannual time scales. Decadal changes in SST appear to be a major  
51 factor in the occurrence of long-term drought, as highlighted by apparent impacts on  
52 precipitation of the late 1990s “climate shifts” in the Pacific and Atlantic SST. Key  
53 remaining research challenges include: (i) better quantification of unforced and forced  
54 atmospheric variability as well as land/atmosphere feedbacks, (ii) better understanding of  
55 the physical basis for the leading modes of climate variability and their predictability, and  
56 (iii) quantification of the relative contributions of internal decadal SST variability and  
57 forced climate change to long-term drought.

58 **1. Introduction**

59 Drought, which can occur in almost any region of the world, is one of the most  
60 destructive natural hazards faced by society. Some of the most dire concerns associated  
61 with climate change are associated with possible changes in drought frequency and  
62 severity, although regional drought projections often show large uncertainties (e.g.,  
63 Seneviratne et al. 2012a; Orłowsky and Seneviratne 2013).

64

65 A substantial amount of research and operational effort has been devoted to drought.  
66 Many drought research studies have focused on particular regions or selected events,  
67 whereas others have examined the global distribution of droughts, their forcing factors,  
68 and their predictability. Efforts in operational environments now routinely assess current  
69 and future drought conditions over a variety of temporal and spatial scales. This broad  
70 range of activities, as well as many drought impact studies, suggests a need to document  
71 our collective understanding of and capabilities to predict drought. A synthesis of current  
72 understanding would help people everywhere benefit as much as possible from existing  
73 research and operational capabilities, through, for example, improved decision support  
74 and drought mitigation.

75

76 The Global Drought Information System (GDIS)<sup>1</sup> addresses these issues. The overall goal  
77 of GDIS is to provide coordinated information, monitoring, and prediction of drought

---

<sup>1</sup> The GDIS was developed as one of the key recommendations of a WCRP workshop on “Drought Predictability and Prediction in a Changing Climate: Assessing Current Knowledge and Capabilities, User Requirements and Research Priorities,” that was held on 2-4 March 2011 in Barcelona, Spain ([http://drought.wcrp-climate.org/workshop/ICPO\\_161\\_WCRP\\_Report.pdf](http://drought.wcrp-climate.org/workshop/ICPO_161_WCRP_Report.pdf)). The capabilities and requirements of the GDIS were further scoped out at a second workshop held in Frascati, Italy on 11-13 April 2012: (<http://www.clivar.org/organization/extremes/resources/dig>). A third workshop, “An

78 worldwide in a user-friendly manner. One of GDIS's objectives is to assess our current  
79 understanding of drought and our ability to predict it, thereby identifying research gaps.  
80 The present special collection of regionally-focused summary articles stems from this  
81 component of GDIS. Each article can stand on its own as an important contribution to  
82 drought research.

83

84 It is also important, of course, to place these summary articles into context and to  
85 synthesize some of their findings. This is the goal of the present overview article. To  
86 make it tractable, we focus primarily on understanding the role of SST in driving  
87 meteorological drought, although some attention is also paid to other drivers as well as  
88 temperature anomalies. Furthermore, some of our discussion will focus more generally  
89 on seasonal-scale precipitation deficits, given that meteorological droughts can be  
90 considered extreme manifestations of such deficits – indeed, the level of deficit required  
91 to define a meteorological drought is not set in stone. In discussing such deficits  
92 generally, we make the implicit assumption that if a given set of conditions (as identified  
93 in this paper) leads to a seasonal precipitation deficit, then a more extreme version of  
94 these conditions would lead to a more extreme deficit and thus potentially a true  
95 meteorological drought. That is, we make the assumption that uncovering the sources of  
96 precipitation deficits on seasonal timescales is tantamount to uncovering the sources (if  
97 conditions therein were stronger) of meteorological drought.

98

---

International Global Drought Information System Workshop: Next Steps”, was held in Pasadena on the Caltech campus 10-13 December 2014, and focused on reviewing the GDIS special collection papers, and developing the necessary next steps required for moving forward with an experimental real time global drought monitoring and prediction system (<http://www.wcrp-climate.org/gdis-wkshp-2014-about>).

99 In this paper we do not address how meteorological drought propagates to agricultural or  
100 hydrological droughts, or how soil moisture feedbacks, temperature changes, or human  
101 water use act to maintain or even amplify the different types of drought, though these  
102 issues are addressed to varying degrees in the articles of this GDIS collection.

103

104 Such a focus does not come without limitations; for example, the impact of long-term  
105 evapotranspiration changes induced by temperature and radiation changes (e.g., from  
106 climate change) may turn out to be as important as (if not more important than)  
107 precipitation changes in some regions in producing soil moisture and streamflow deficits  
108 at longer time scales (e.g., Cook et al. 2014; Cook et al. 2015). For example, Cook et al.  
109 (2014) used CMIP5-driven Palmer Drought Severity Index (PDSI) and Standardized  
110 Precipitation-Evapotranspiration Index (SPEI, Vicente-Serrano et al. 2010) drought  
111 estimates to show that, while robust regional changes in hydroclimate are primarily  
112 organized around regional changes in precipitation, increased potential  
113 evapotranspiration (PET) computed with the Penman-Monteith approach nearly doubles  
114 the percentage of global land area projected to experience significant drying based on  
115 these indices by the end of the 21st-century. Nevertheless, Sheffield et al. (2012), in  
116 addressing whether such impacts of increased PET are already evident in recent  
117 observationally-driven PDSI trends, found that global drought has changed little over the  
118 past 60 years (see also Seager and Hoerling 2014 for a discussion of regional  
119 differences), indicating that the focus here on precipitation deficits allows us to address  
120 much of the overall drought problem in current climate. Table 1 provides further

121 evidence that such a focus is justified, showing for our selected regions (see Section 3)  
122 generally high correlations between precipitation and either the PDSI or soil moisture.

123

124 We start by providing an overall scientific context for drought through an examination of  
125 the global drivers of precipitation and temperature changes on interannual and decadal  
126 time scales (Section 2). Next, we relate these and other factors to drought in different  
127 regions, highlighting implications for predictability and prediction (Section 3). Section 4  
128 provides some concluding remarks.

129

## 130 **2. Overview of Large Scale Factors**

131 Here we review the large-scale or the ultimate (as opposed to the proximate) causes of  
132 meteorological drought - the processes responsible for the long-term disruptions of local  
133 and regional precipitation-producing phenomena. These processes often act over large  
134 distances via various large-scale atmospheric motions such as the Hadley and Walker  
135 circulations, Rossby waves, and other atmospheric teleconnection patterns. The forcing  
136 for some of these large-scale motions is known to include sea surface temperature  
137 anomalies (SST), land (especially soil moisture) feedbacks, aerosols, and other natural  
138 and anthropogenic changes in radiative forcing such as those associated with global  
139 warming. These forcings are important because they may provide some degree of  
140 drought predictability (e.g., Smith et al. 2012). It must be kept in mind, however, that  
141 there is a substantial unforced (i.e., driven by processes internal to the atmosphere)  
142 element to the large-scale motions that significantly limits our ability to predict drought  
143 at the longer leads.

144

145 The various papers in the GDIS drought special collection assess, from a regional  
146 perspective, the global processes associated with meteorological drought. We summarize  
147 these findings here, while also providing some additional background on climate change  
148 aspects and regarding meteorological drought on the European continent. In addition, to  
149 provide a global framework for our discussion and synthesis, we include a model-based  
150 assessment of the dominant large-scale forcing of meteorological drought on seasonal  
151 and longer time scales – the response of the atmosphere to SST anomalies (e.g., Hoerling  
152 and Kumar 2003; Schubert et al. 2004; Seager et al. 2005). This assessment is based on  
153 AMIP-style simulations using prescribed SSTs (see Appendix A), with 5 different state-  
154 of-the-art global climate models; results are presented as combined (rather than  
155 individual model) statistics. We provide the model results in each subsection partly to  
156 assess their consistency with the findings of the individual special issue GDIS papers.  
157 The model results also provide insight into the spatial coherence and seasonality of the  
158 forced responses. In examining these results, we must keep in mind that their usefulness  
159 may be limited by model deficiencies and by the limitations imposed by employing SST-  
160 prescribed, integrations.

161

162 The link between drought and remote SST anomalies is complicated by the fact that there  
163 are different definitions of drought reflecting a wide range of societal (e.g., health, water  
164 quality, political), economic (e.g., agriculture, water supply, transportation, recreation)  
165 and ecosystem (e.g., fish, wildlife, wetlands, biodiversity, forest fires) impacts<sup>2</sup>. All of  
166 these definitions are important. Nevertheless, we focus here on the primary

---

<sup>2</sup> More on impacts can be found at <http://drought.unl.edu/Planning/Impacts.aspx>

167 meteorological quantity associated with dry conditions, namely, precipitation. In  
168 addition, we also consider conditions in near surface air temperature, which can affect  
169 surface drying through increased evaporative demand in warmer air, although the latter  
170 can also result from soil drying associated with meteorological drought itself (e.g.  
171 Mueller and Seneviratne 2012; Sheffield et al. 2012; Yin et al. 2014). We begin with an  
172 overview of the interannual variability of both precipitation and temperature.

173

174 Figure 1 shows the land regions where SST anomalies are expected to influence annual  
175 mean precipitation and two meter (2 m) air temperature, based on the five Atmospheric  
176 General Circulation Models (AGCMs: 12 ensemble members for each) forced with  
177 observed SST over the period 1979-2011. (See Appendix A for descriptions of the  
178 models and simulations). The base maps show the fraction of the total interannual  
179 variance that is forced by SST. Focusing on precipitation (Fig. 1a), we see that the ratios  
180 outside the tropics (poleward of +/- 30° latitude) are generally quite small ( $< 0.2$ )<sup>3</sup>;  
181 outside the tropics, much of the interannual variability is unforced by SST and is  
182 therefore likely to be unpredictable from SST forcing at interannual time scales. This is  
183 for instance the case in northern Eurasia, central Europe as well as central and eastern  
184 Canada. We note nonetheless that (agricultural and hydrological) drought predictability  
185 in these regions may be arising from year-to-year memory in soil moisture and/or snow  
186 pack, or possibly interannual changes in radiative forcing, aspects that we do not consider  
187 in the present review. The largest fractions of interannual precipitation variability  
188 explained by SST in the midlatitudes occur over the U.S. southern Great Plains,

---

<sup>3</sup> We note that values of the ratio greater than 0.06 are statistically significant at the 1% level based on a F-test following Zwiers et al. (2000).



189 southwest Asia, parts of Australia and South America. Values exceed 0.3 primarily in  
190 tropical land areas, including northwest South America, Indonesia, Central America,  
191 southeast Asia, southwestern India, and eastern Africa. The fractions for 2m temperature  
192 (Fig. 1b) are generally considerably larger than those for precipitation. Some regions in  
193 the extratropics show values exceeding 0.4 (e.g., southern US Great Plains and Mexico).  
194 Nevertheless, the largest values are again confined to the tropical regions of Africa,  
195 southern Asia, Indonesia and much of the northern half of South America, with values  
196 sometimes exceeding 0.7.

197 El Niño/Southern Oscillation (ENSO) is a key player in the development of precipitation  
198 deficits in many regions of the world (e.g., Ropelewski and Halpert 1987). Figure 1, in  
199 addition to showing the fraction of interannual variance forced by SST, shows how SST  
200 is correlated with precipitation (Fig. 1a) and T2m (Fig. 1b) within selected regions (small  
201 inserts)<sup>4</sup>; the patterns show a clear link to ENSO and to SST in general. We will refer to  
202 these maps as we review the results from the individual contributions to this special  
203 collection.

204 A number of regions of the world have suffered multi-year drought (e.g., beyond the  
205 ENSO time scale), and one may wonder whether such droughts result from naturally  
206 occurring decadal modes of variability (e.g., the Atlantic Multi-decadal Oscillation or

---

<sup>4</sup> We emphasize that these are meant to be summary results. As we shall see in section 3, there are in some cases considerable variations in SST connections within a box and between seasons. For example, the western portions of East Africa tend to have a JJAS rainfall maximum, and El Niño is tied to drought. Further east (eastern Ethiopia, Kenya, Somalia) the rainy season is bimodal with drought associated with La Niña (and its influence on Indian Ocean SSTs) during boreal fall. The ENSO signal reverses sign between East and Southern Africa as well, with 15° south frequently considered the northern limit of the southern African region. Some of these seasonal and regional differences are discussed in section 3.

207 AMO and Pacific Decadal Oscillation or PDO), from decadal changes in the relationships  
208 between interannual modes of variability (e.g., ENSO and Atlantic Niños; Losada et al.  
209 2012), from global warming (Mohino et al. 2011a), or from no mechanism at all, i.e.,  
210 from a simple random sequence of dry years generated from internal atmosphere  
211 variability. In Figure 2 we provide a global depiction of the changes that have occurred  
212 over the last three decades in the tails of the probability distributions of 2m temperature  
213 and precipitation based on the same set of AGCM runs used to produce the results in  
214 Figure 1. Here we show how the probability of exceeding (or falling short of, in the case  
215 of precipitation) a particular critical value  $x_c$  has changed between the first and last  
216 fifteen years of the record. Because we are focusing on extreme years,  $x_c$  is chosen to be  
217 the 2.5% value based on all 33 years – i.e., the value that would be exceeded (or fallen  
218 short of) on average only 2.5% of the time. The last three decades, we note, are  
219 characterized by both global warming and shifts in the AMO and PDO (Figure 3), so  
220 anthropogenic forcing and natural variations may both contribute significantly to  
221 observed regional changes between these two periods.

222

223 In regard to precipitation (Fig. 2a), the models indicate that much of the United States has  
224 experienced an increase in the probability of extreme dry years during the last three  
225 decades (particularly the central Plains). Here the shift is 1 to 1.5 times the  
226 climatological probability of 2.5%. The shift is clear in the probability density functions  
227 (pdfs) provided in the insert. As we shall see next, this shift reflects forcing by SST with  
228 a strong decadal component and does not necessarily reflect a long-term trend. In fact, if

229 a longer time period is considered, the United States (especially the central part of the  
230 country) has generally experienced wetter conditions compared to the 1950s (e.g., Wang  
231 et al. 2009; Seneviratne et al. 2012; Hartmann et al. 2013; Greve et al. 2014). As Wang  
232 et al. 2009 showed however, even for this longer time period the precipitation “trend” is  
233 still dominated by SST forcing with decadal time scales.

234 Parts of Indochina and southeastern China also see an increase in the probability of  
235 extreme dry years. In contrast, northeastern South America shows a substantial decrease  
236 in the probability of dry years over the last three decades, though with little change in the  
237 probability of extreme wet years (see insert). The tropical west coast of Africa, the Sahel,  
238 and northeastern Russia also show a reduction in the probability of extreme dry years.  
239 The pdf characterizing precipitation in northeastern Africa shows no shift in the peak, so  
240 that the changes in the pdf occur primarily in the tails. In general, for the Northern  
241 Hemisphere during the last three decades, the high latitudes show a tendency for a  
242 reduction in the probability of dry years, whereas the middle latitudes (including parts of  
243 Europe, southern Asia and the U.S.) show a tendency for an increase in the probability of  
244 dry years. In the Southern Hemisphere, the probability of extreme dry years is increased  
245 in parts of southern Africa, Australia and southern and western South America and  
246 mostly decreased in tropical regions.

247 Relative to precipitation, the results for 2m temperature (Figure 2b) are more  
248 homogenous, with almost all regions of the world showing an increase in the probability  
249 of very warm years over the last three decades (see also Hartmann et al. 2013). Regions  
250 where the increase in probability exceeds twice the climatological probability of 2.5%

251 include the south central U.S., Mexico, northwestern South America, eastern Canada,  
252 parts of Europe, southern Asia, Japan, tropical and northern Africa, Indonesia, and  
253 southern Australia. Only northeastern South America and western Canada show  
254 substantial regions with little increase (and even some scattered regions of decrease) in  
255 the probability of warm years. The inserts show that these changes largely result from a  
256 shift in the mean rather than from a change in the shape of the pdfs for the analyzed  
257 regions.

258 Figure 3 compares the simulated and observed mean changes between the two 15 year  
259 periods. The model results show warming everywhere except over northwestern North  
260 America and northeastern South America, with the strongest warming occurring in the  
261 Northern Hemisphere. The model results are generally consistent with the observed  
262 temperature changes, although they are smoother due to being an average over 60  
263 ensemble members. There are also strong similarities between the simulations and  
264 observations in the precipitation differences, with both difference maps showing  
265 decreases over the U.S. and increases over northern South America, northern Australia,  
266 northern Eurasia, and central Africa. Some differences in the estimated precipitation  
267 changes, however, do appear, including over central South America (observed decreases  
268 not found in the simulations), India, and southeast Asia. The extent to which these reflect  
269 model deficiencies or sampling differences associated with unforced internal atmospheric  
270 noise is unclear. Overall, the changes are consistent with the changes in the pdfs  
271 discussed earlier. They appear to reflect, in part, a response to SST changes linked to the

272 PDO, the AMO, and a warming trend (Fig. 3, see also Schubert et al. 2009), as well as  
273 possible direct impacts on the atmosphere from increasing GHGs<sup>5</sup>.

### 274 **3. Causes of Meteorological Drought by Region**

275 We now provide a more in-depth discussion of meteorological drought for specific  
276 regions. While much of the discussion is condensed from the individual contributions to  
277 this special collection, we also present relevant results from the aforementioned SST-  
278 forced AGCM simulations, as well as results from other key studies where necessary to  
279 address issues not covered by the individual contributions.

280

281 We begin by providing in Figure 4 a brief assessment of the ability of the models to  
282 produce the observed annual cycle of precipitation in each of the selected regions (see the  
283 boxes in Figures 5-8 for the definitions of the regions). This is also meant to facilitate the  
284 following discussion about the links to SST, by giving the reader an assessment of the  
285 timing of the wet and dry seasons in each region. Overall, the models do a reasonable job  
286 in reproducing the observed annual cycle, though the peak rainfall tends to be  
287 underestimated especially in the tropical land regions (N. South America/Central  
288 America, Southern Eurasia, Indonesia)<sup>6</sup>. It is noteworthy that the Central/South  
289 American region (Figure 4a) shows some evidence of the well-known mid summer  
290 drought found over Mexico and Central America (e.g., Magaña et al. 1999) – something  
291 that is also reproduced in the model results. We also note that the spatial averaging tends  
292 to hide any regional differences. This is especially true for the east African region which

---

<sup>5</sup> All the AGCMs (except for CCM3) were forced with observed GHGs (Appendix A).

<sup>6</sup> We note that including the ocean points when computing the area averages of the precipitation in these regions produces much closer agreement between the observations and model results (not shown), indicating the underestimation of the precipitation is confined to the land areas.

293 shows a rather flat annual cycle (Figure 4b), despite having local rainfall regimes that  
294 include unimodal (JJA and DJF maxima) and bimodal (MAM, OND maxima) annual  
295 cycles (see section 3.3).

296

### 297 *3.1 North America*

298 The occurrence of precipitation deficits over North America on annual time scales is  
299 predominantly associated with SST variability in the tropical Pacific (e.g., Seager et al.  
300 2005), with some contribution from SST variability in the Atlantic (e.g., Schubert et al.  
301 2009). Figure 1a shows that precipitation deficits are largely tied to La Nina conditions,  
302 with the largest impacts in the southern Great Plains and Northern Mexico. La Nina  
303 conditions also lead to warming across the Southern Plains and much of the southeast,  
304 whereas El Nino conditions are associated with warming over Alaska and northwestern  
305 Canada (Fig. 1b).

306

307 These results are consistent with the in-depth assessment of the causes of North  
308 American drought carried out by Seager and Hoerling (2014). Using a subset of the  
309 climate models underlying Figure 1, Seager and Hoerling (2014) find that SST forcing of  
310 annual mean precipitation variability accounts for up to 40% of the total variance in  
311 northeastern Mexico<sup>7</sup>, the southern Great Plains and the Gulf Coast states but less than  
312 10% in central and eastern Canada. They further find that, in addition to the tropical  
313 Pacific, tropical North Atlantic SST contributes to the forcing of annual mean

---

<sup>7</sup> Mexico will be discussed further in the following section.

314 precipitation and soil moisture in southwestern North America and the southern Great  
315 Plains.

316

317 Seager and Hoerling (2014) find that SST forcing was indeed responsible for multiyear  
318 droughts in the 1950s and at the turn of the 21<sup>st</sup> Century. Attribution to SST patterns,  
319 however, is not always straightforward. Wang et al. (2014) highlight how the responses  
320 over North America to SSTs in different ocean basins can reinforce each other or cancel  
321 out, complicating the analysis of SST impacts. Atmospheric internal variability also  
322 muddies the signal; internal atmospheric variability can contribute significantly to  
323 extreme droughts, especially on shorter (monthly) time scales (Seager et al 2014a;  
324 Hoerling et al. 2014; Wang et al. 2014). For example, the most extreme phase of the  
325 Texas drought in 2011 was largely unforced by SST, and the central Plains drought of  
326 2012 showed almost no contribution from SST forcing.

327

328 Figure 5 (left panels) shows, for the United States and northern Mexico, the seasonality  
329 of the link between precipitation and SST, as determined from the model simulations.  
330 The most striking aspect of this seasonality is the strong ENSO connection for all seasons  
331 except JJA, though the strong connection in MAM is not supported by the observations  
332 (see Fig. B5). Summertime precipitation is negatively correlated with tropical Atlantic  
333 SST, a result consistent with Kushnir et al. (2010) and Wang et al. (2008), who showed  
334 that a larger Atlantic Warm Pool leads to a suppressed Great Plains Low Level jet and  
335 associated reduced Central U.S. precipitation. On the other hand, summertime  
336 precipitation is positively (though weakly) correlated with SST along the west coast of

337 North America extending into the central tropical Pacific, with a structure reminiscent of  
338 the PDO. The link to the Indian Ocean also has substantial seasonality, with positive  
339 correlations during DJF and MAM and negative correlations extending westward from  
340 the warm pool into the eastern Indian Ocean during SON.

341

342 Seager and Hoerling (2014) show that, during the early 21st Century, natural decadal  
343 variations in tropical Pacific and North Atlantic SSTs have contributed to a dry regime  
344 for the U.S. (see also Fig. 3). Since the mid 1990s both the PDO and the AMO have  
345 gone through striking decadal transitions (Figure 3) to a cold tropical Pacific-warm North  
346 Atlantic that is “ideal” for North American drought (Schubert et al. 2009). Figure 2  
347 indicates that in the southern plains region, the drier regime is associated with a  
348 substantial increase in the probability of extreme dry years. In addition, Seager and  
349 Hoerling (2014) note that long-term changes caused by increasing trace gas  
350 concentrations are now contributing to a modest signal of soil moisture depletion, mainly  
351 over the American Southwest, thereby prolonging the duration and severity of naturally  
352 occurring droughts.<sup>8</sup>

353

354 Understanding the extent to which precipitation and air temperature variability is  
355 determined by SST forcing (potentially providing predictability) and internal atmospheric  
356 variability (providing no predictability on seasonal and longer time scales) is an  
357 important research challenge (e.g., Wang et al. 2014). Recently the 2011-14 California  
358 drought has been linked to a localized warm SST anomaly in the western tropical Pacific

---

<sup>8</sup> Water pumping is another source of drying in the SW US.



359 (Seager et al. 2014c; Hartmann 2015), which raises the important issue of forcing of  
360 drought over North America by Pacific SST anomaly patterns other than ENSO. The  
361 contribution of soil moisture to the variability is also still poorly understood, as reflected  
362 by the substantial differences in the strength of land-atmosphere feedback and soil  
363 moisture memory simulated by current climate models (e.g., Koster et al. 2004;  
364 Seneviratne et al. 2006). Also poorly understood is the nature and predictability of the  
365 unforced component (e.g., internal atmospheric variability associated with Rossby waves  
366 and other atmospheric teleconnections, especially during the summer).

367

368 Regarding changes under enhanced greenhouse gas concentrations and global warming,  
369 the additional forcing of increasing radiation could lead to enhanced evapotranspiration  
370 during drought events. Climate projections for the end of the 21<sup>st</sup> century suggest a robust  
371 increase of soil moisture drying in the southern United States and Mexico, while signals  
372 for accumulated precipitation deficits are less robust across climate models (Orlowsky  
373 and Seneviratne 2013). However, historical records do not yet suggest a detectable signal  
374 in North America, either in precipitation or precipitation-evapotranspiration (Hartmann et  
375 al. 2013; Greve et al. 2014). How the SST impacts may change in a warming world is  
376 largely unknown.

377

### 378 *3.2 Latin America*

379 Figure 1 shows that SST impacts on temperature and precipitation are strong over  
380 northern South America; these signals are largely associated with ENSO and tropical  
381 Atlantic variability (e.g., Mechoso and Lyons 1988; Saravanan and Chang 2000; Giannini

382 et al. 2004). Via this connection, this region may see substantial improvements in  
383 seasonal prediction skill as climate models improve (e.g., Folland et al. 2001; Goddard et  
384 al. 2003). In Central America, as in northern South America, precipitation is correlated  
385 negatively with tropical Pacific SST and positively with tropical Atlantic SST. Indeed,  
386 the extent to which the Atlantic signals are independent of ENSO is still not fully  
387 quantified (e.g., Chang et al. 2003). Extreme droughts in northeast Brazil have been  
388 linked to very strong El Niño events (McCarthy et al. 2001). Conversely, western  
389 Amazon droughts depend on tropical North Atlantic SST anomalies more than on ENSO  
390 (Marengo et al 2008). Further analysis demonstrated that the North Tropical Atlantic  
391 influence is largest during dry season droughts in the southern Amazon, but ENSO still  
392 has a stronger influence during the wet season for the entire basin (Yoon and Zeng 2009).

393

394 Figure 1 also shows that relatively strong signals for precipitation over South America  
395 extend south along the west coast which shows enhanced precipitation associated with La  
396 Niña conditions. Relatively high temperature signals along the west coast extending  
397 southward into northern Chile are associated with positive correlations with El Niño.  
398 The east coast over southern Brazil and Uruguay, including northern and central  
399 Argentina (much of the La Plata basin), has reduced precipitation associated with La  
400 Niña conditions (Diaz et al. 1997; Fig. 1a). According to McCarthy et al. (2001), during  
401 La Niña events Chile and central-western Argentina, exhibit negative anomalies of  
402 rainfall and snowfall leading to reduced summer streamflow.

403

404 Figure 5 illustrates the seasonality of the link to SST over northern South America and

405 Central America (middle column) and over central-southern South America (right  
406 column). For the former region, the aforementioned link to the El Niño cycle is weakest  
407 in March-April-May (MAM), and the link to the tropical Atlantic is strongest during  
408 June-July-August (JJA) and September-October-November (SON). On the other hand,  
409 Cazes-Boezio et al. (2003) show that the ENSO impact on precipitation in Uruguay  
410 occurs primarily during austral spring (October–December), but is almost absent during  
411 peak summer (January –February), followed by weak impacts during March-July. This is  
412 not inconsistent with our much larger central-southern South American region (and with  
413 somewhat different definitions of the seasons), which is characterized by reduced  
414 (enhanced) precipitation in association with La Niña (El Niño) conditions for all seasons  
415 except December-January-February (DJF), when correlations with SST are negligible.  
416

417 While droughts in southeastern South America exhibit a strong dependence on La Niña  
418 (cold Pacific), a warm North Tropical Atlantic can help define the shape and intensity of  
419 the drought episodes (Seager et al. 2010; Mo and Berbery 2011). Notably, the effect of  
420 land surface-atmosphere interactions, in the form of soil moisture-precipitation coupling,  
421 is essential in the development of drought in southern South America (Xue et al. 2006;  
422 Wang et al. 2007; Ma et al. 2010; Sörensson and Menéndez 2011). Barreiro and Diaz  
423 (2011) noted that improved seasonal forecasts over South America require the proper  
424 representation of the teleconnection processes and regional land–atmosphere interactions  
425 need to be adequately resolved. Müller et al. (2014) showed that during the severe 2008  
426 drought in southern South America, a realistic representation of land surface biophysical  
427 properties leads to a better depiction of surface-atmosphere processes that consequently

428 reduces model biases and eventually contributes to improved prediction skill of droughts.

429

430 McCarthy et al. (2001) note that in Central America, topography influences the ENSO  
431 impacts; during El Niño years, the Pacific side is characterized by reduced precipitation,  
432 while some parts of the Caribbean side have above normal rain. They also note that over  
433 Colombia, El Niño events are associated with reductions in precipitation, streamflow, and  
434 soil moisture, whereas La Niña is associated with heavier precipitation and floods  
435 (Poveda and Mesa, 1997), especially during December-January. El Niño also tends to  
436 bring large positive precipitation anomalies to the eastern part of the Andes, Ecuador, and  
437 northern Peru.

438

439 Future climate scenarios produced by regional downscaling suggest a precipitation  
440 decrease over the tropical region of South America, with an increase over the subtropical  
441 areas (Sanchez et al. 2015). In relation to extremes, climate change scenarios for South  
442 America suggest an increase of dry spells, with more frequent warm nights (Marengo et  
443 al. 2009).

444

445 3.3 *East Africa*

446 Lyon (2014) provides a review of the regional and large-scale SST and atmospheric  
447 circulation patterns associated with meteorological drought in East Africa on seasonal  
448 and longer time scales. Analysis of drought in the region is complicated by local rainfall  
449 regimes that generally consist of unimodal (JJA and DJF maxima) and bimodal (MAM,  
450 OND maxima) annual cycles. On seasonal-to-interannual time scales, ENSO is the  
451 largest source of seasonal rainfall variations, but depending on season and location, it has  
452 opposite effects: La Niña is frequently associated with drought during the OND “short  
453 rains” in the central and eastern areas of the Greater Horn (this is not well captured  
454 captured by most of the models – see Figures 6 and B1), whereas El Niño is linked to  
455 deficient rainfall during boreal summer in locations further west having a unimodal  
456 annual cycle (consistent with Figure 6). Particularly for the short rains, the Indian Ocean  
457 plays a critical role in mediating the impact of ENSO, with the development of a west-  
458 east Indian Ocean SST anomaly dipole pattern (IOD) being closely associated with  
459 rainfall variations (see also Figure 6). ENSO, however, is associated with at most roughly  
460 25% of interannual variations in East African rainfall (consistent with Figure 1).

461

462 In observations, interannual variations in MAM “long rains” (Funk et al. 2008; Lyon and  
463 DeWitt 2012) in East Africa do not show statistically significant correlation with SSTs in  
464 any ocean basin (generally consistent with Figure 6, though the models do show positive  
465 correlations with SST in the western Indian Ocean). At longer time scales, AMIP-style  
466 model runs do tend to capture the decline in the East African long rains associated with  
467 the shift in Pacific SSTs towards the cool phase of the PDO in 1998-99 (Lyon 2014,

468 Yang et al. 2014, see also Figures 3 and 9). The models may thus respond more to  
469 decadal, rather than interannual, variations in SSTs. Liebmann et al. (2014) suggest this  
470 result may be tied to the relative magnitudes of multidecadal SST fluctuations relative to  
471 interannual variability.

472

473 On longer timescales, there is growing concern over an observed increase in the  
474 frequency of drought, primarily during the MAM long rains. This increase has had dire  
475 impacts across the Greater Horn, with the most recent and severe drought in 2010-11  
476 helping to trigger a humanitarian crisis and contributing to the fatalities of tens of  
477 thousands of people. The increase in drought frequency has raised concerns about the  
478 possible role of anthropogenic climate change. Paradoxically, the consensus of climate  
479 model projections is for the region to become wetter during the current century in  
480 response to anthropogenic greenhouse gas forcing (IPCC 2007). Lyon et al. (2013), Lyon  
481 (2014) and Yang et al. (2014) provide evidence that the recent rainfall decline is  
482 substantially driven by natural, multi-decadal variability, a result consistent with our  
483 model simulations (Figure 9). Consistent with Lyon and DeWitt (2012), subsequent  
484 studies by Hoell and Funk (2013, 2014) suggest that long-term anthropogenic warming of  
485 the western Pacific may further enhance the equatorial SST gradient associated with the  
486 cold phase of the PDO and thus also enhance drying in East Africa during MAM. As to  
487 whether East Africa will become wetter or drier as a result of anthropogenic forcing,  
488 Yang et al. (2014) caution that most coupled climate models do not properly capture  
489 either the observed annual cycle of rainfall in East Africa or the observed relationship  
490 between seasonal rainfall variations and SSTs in different basins (particularly the Indian

491 Ocean), calling into question the reliability of climate projections in East Africa. Lyon  
492 (2014) concludes that the hydroclimatic response of East Africa to anthropogenic climate  
493 change remains an open question and that more research is needed to better understand  
494 the physical processes associated with rainfall variability of the region across multiple  
495 timescales.

496

### 497 *3.4 West Africa and Sahel*

498 Rodríguez-Fonseca et al. (2015) focus on rainfall variability across multiple timescales in  
499 West Africa and the Sahel. They conclude that SST variations are largely responsible for  
500 rainfall variability in the region. Land surface processes and aerosols including those  
501 from volcanic eruptions modulate the SST influence.

502

503 The left column in Fig. 6 indicates a strong seasonality in the correlation between West  
504 African (including western Sahel) rainfall and SST in the simulation by the five models  
505 with prescribed SST corresponding to the observed over the period 1979-2011. During  
506 the rainy season (JJA), increased precipitation over West Africa is associated with colder  
507 SST in the eastern tropical Pacific and northern Indian Ocean, and with warmer SST in  
508 the tropical Atlantic/Gulf of Guinea. During the dry season (DJF), when climatological  
509 precipitation is small, increased precipitation is associated with warmer SST in the  
510 tropical Atlantic/Gulf of Guinea, as well as in the tropical North Atlantic and central  
511 tropical Pacific. Correlations are weaker and less organized in the Pacific during MAM,  
512 and little connection with SST is apparent during SON.

513

514 Other experiments using AGCMs with prescribed SSTs in individual ocean basins have  
515 provided additional insight. During the wet season, warm equatorial SST anomalies  
516 corresponding to a warm Atlantic Niño (Rodríguez Fonseca et al. 2009) are associated  
517 with precipitation increases over the Gulf of Guinea and weaker decreases over the Sahel.  
518 The impact of a Pacific warm event varies during the season. In the early part of the  
519 season (May-June) warming of the equatorial Pacific reduces rainfall over the Gulf of  
520 Guinea and enhances it over the Sahel. In the late part of the wet season (July-August)  
521 warming of the equatorial Pacific reduces rainfall over the Sahel. In the seasonal mean,  
522 the negative effects of the Pacific Niños in the late season prevail over the positive ones  
523 in the early period as shown in Fig. 6.

524

525 Rodríguez-Fonseca et al. (2015) discuss a unique aspect of the West African rainfall  
526 variability at interannual time scales: its links with the variability of tropical SSTs have  
527 shown non-stationary features (see also Rodríguez-Fonseca et al. 2011 and Mohimo et al.  
528 2011b). Pacific cold events and Atlantic warm events tend to appear simultaneously after  
529 the 1970's (Rodríguez-Fonseca et al. 2009). AGCM experiments demonstrate that, during  
530 this period, the impacts of simultaneous SST anomalies in the Indo-Pacific and Atlantic  
531 on Sahel rainfall tend to cancel each other such that the north-south dipole in rainfall  
532 anomalies over West Africa expected from Atlantic SST anomalies only does not appear  
533 in the observations (Losada et al. 2012).

534

535 Analysis of observational data and model results has provided clues on the mechanisms  
536 at work in the connections described above. Anomalous warming of the southern tropical



537 Atlantic enhances ascent over the Gulf of Guinea and descent over the Sahel. A warming  
538 in the Pacific and Indian Oceans generates equatorial Rossby waves that contribute to  
539 subsidence over the Sahel and thus to reduce regional precipitation. Also, Mediterranean  
540 warm events are linked to increased moisture flux convergence over the Sahel.  
541

542 Decadal SST variability and global warming are also relevant to Sahelian drought. In recent  
543 decades the Sahel has been recovering from a devastating drought in the 1970s and 80s. It has  
544 been suggested that a special combination of three different modes of SST variability (the global  
545 warming trend, the positive phase of the Inter-decadal Pacific Oscillation, and the negative phase  
546 of the Atlantic Meridional Oscillation, or AMO) led to this drought (Mohino et al., 2011a).

547 Vegetation dynamics has been contributing to regional climate persistence (e.g., Zeng et al.  
548 1999). The recovery from the drought appears to be driven by SST also, as a similar feature is  
549 obtained in SST-forced model simulations. Regarding global warming, Rodríguez-Fonseca et al.  
550 (2015) note that, while rainfall projections have a large spread, models do show a tendency for  
551 slightly wetter conditions over the central Sahel and drier conditions over the west. The onset of  
552 the rainy season is projected to be delayed, especially over West Africa, while more abundant  
553 precipitation is expected during the late rainy season.  
554

555 Rodríguez-Fonseca et al. (2015) caution that more research is needed to further support these  
556 model-based findings on the variability of Sahel rainfall. While most models capture, for  
557 example, the link with Mediterranean SSTs, some important teleconnections are still not well  
558 reproduced (e.g., those linked to equatorial Atlantic SSTs and Pacific ENSO; Rowell 2013).

559 Also, coupled atmosphere-ocean general circulation models have great difficulties in correctly

560 reproducing the seasonal cycle and variability of the tropical Atlantic SST (including the Atlantic  
561 Equatorial mode; Richter 2015) and Pacific (e.g. Mechoso et al. 1995).

562

### 563 *3.5 The Middle East and Southwest Asia*

564 Barlow et al. (2015) provide a comprehensive review of current understanding of drought  
565 in the Middle East and Southwest Asia – a region that is water-stressed, societally  
566 vulnerable, and prone to severe droughts. They note that this understanding is still at an  
567 early stage, though it appears that large-scale climate variability, particular La Niña in  
568 association with a warm western Pacific, contributes to region-wide drought, including  
569 the two most severe droughts of the last fifty years (1999-2001 and 2007-2008). Barlow  
570 et al. (2015) provide a schematic for those two years indicating how La Niña-related  
571 SSTs and a warm western Pacific led to wave responses that affected vertical motion,  
572 moisture flux and storm tracks in the region. They note that the North Atlantic Oscillation  
573 (NAO), the AMO, and the Atlantic SST tripole pattern also influence the region, though  
574 the strength of the teleconnections varies considerably within the region, and the  
575 temporal stability of the relationships is somewhat uncertain.

576

577 Figure 1 (top panel) highlights the role of ENSO (and perhaps the PDO) in influencing  
578 drought in Southwest Asia on annual time scales. This result shows some model  
579 dependence but appears to be consistent with observations (Figure B2). Figure 7 (left  
580 column) shows that there is a strong seasonality to the precipitation-SST connection in  
581 this region, with the strongest correlations in MAM (La Niña, together with a cool  
582 tropical Indian Ocean and cool tropical North Atlantic, is apparently conducive to

583 drought conditions then) and similar, though somewhat weaker (especially in the tropical  
584 Indian Ocean) correlations in DJF. These two seasons comprise the wet season for most  
585 of the region, associated with synoptic precipitation (Barlow et al. 2015). Warm season  
586 precipitation is important in Pakistan and the southern coast of the Arabian Peninsula,  
587 associated with the Indian monsoon and the ITCZ. During JJA the link to SST changes  
588 sign in the tropical Pacific, so that reduced precipitation is linked to warm tropical Pacific  
589 SSTs together with cold SSTs in the tropical Atlantic. SON shows the beginnings of the  
590 cold-season link to ENSO, with a coherent ENSO pattern extending from the western  
591 Mediterranean into Southwest Asia (Mariotti 2007).

592

593 Barlow et al. (2015) note that in the high mountains of the region, snowmelt provides  
594 predictability for peak river flows and potentially for vegetation; vegetation in the region  
595 is closely linked to precipitation and may also play a feedback role. The drying of the  
596 eastern Mediterranean is a robust feature of future projections, as are temperature  
597 increases across the region.

598

### 599 *3.6 East Asia*

600 Zhang and Zhou (2015) review drought over East Asia with a primary focus on China.  
601 They point out that due to the seasonal variation of monsoonal circulation, drought  
602 mostly occurs over North China and Southwest China in spring, with the highest drought  
603 frequency and maximum duration occurring during that season. In early July, drought  
604 tends to occur in the Yangtze River and Huaihe River valleys of China and also Korea  
605 and Japan due to the influence of the Northwestern Pacific subtropical High.

606

607 The interannual variability of East Asian summer (EASM) precipitation is in part  
608 associated with the Pacific-Japan teleconnection pattern, which features a meridional tri-  
609 polar pattern during decaying El Niño summers, with excessive precipitation in central  
610 eastern China along the Yangtze River valley (27.5°N-32.5°N,102°E-120°E) but drier or  
611 even drought conditions in southern (20°N-27.5°N,102°E-120°E) and northern (32.5°N-  
612 45°N,102°E-120°E) China, or vice versa (Huang and Li et al. 2007). This is associated  
613 with an anomalous anticyclone over the western North Pacific forced by the SST  
614 anomalies there and over the Indian Ocean during decaying El Niño summers (Li et al.  
615 2008; Xie et al. 2009; Wu et al. 2009, 2010). The Silk Road teleconnection, a pattern  
616 forced by Indian monsoon heating and characterized by the propagation of a stationary  
617 Rossby wave along the Asian jet in the upper troposphere, also affects East Asia, mainly  
618 North China precipitation (Wu et al. 2003; Ding et al. 2011).

619

620 Drought trends over China since about 1950 are characterized by a zonal dipole pattern,  
621 with an increasing trend over the central part of North China and a decreasing tendency  
622 over Northwest China. The drying and warming trend over North China is associated  
623 with an inter-decadal weakening of the East Asian summer monsoon circulation, which  
624 has been mainly linked to the 1970s phase transition of the PDO from negative to  
625 positive values (Zhou et al. 2009a, 2013). While the weakening of the monsoon  
626 circulation is well reproduced by AMIP-type simulations (Li et al. 2010), the associated  
627 anomalous precipitation change found in observations is poorly reproduced over East  
628 Asia. This is likely in part due to the bias' that exist in simulating the climatological

629 precipitation in this region, resulting from the inability of current relatively coarse global  
630 models to resolve the complex terrain over Asia (Zhou et al. 2008a,b, Li et al. 2015).

631

632 While CMIP5 experiments indicate that aerosols act to weaken monsoon circulation, the  
633 simulated change is much weaker than observed (Song et al. 2014). A 50-70 year  
634 variation in the PDO index appears to be imprinted in century-scale variations of drought  
635 in North China (Qian and Zhou 2014).

636

637 Up to now, most efforts have focused on exploring the prediction skill of East Asian  
638 monsoon precipitation, with few examining drought predictability. Previous studies show  
639 that climate models have limited skill in simulating and predicting the precipitation in  
640 terms of both climatological mean state and interannual variations (Chen et al. 2010;  
641 Zhou et al. 2009b). In contrast, the variability of East Asian monsoon circulation is well  
642 captured (Zhou et al. 2009c; Song and Zhou 2014a). A successful reproduction of the  
643 interannual EASM pattern depends highly on the Indian Ocean–western Pacific  
644 anticyclone teleconnection (Kim et al. 2012; Song and Zhou 2014a,b). Finally, Zhang and  
645 Zhou (2015) note that in climate change projections, most climate models simulate an  
646 increasing drought frequency and intensity over East Asia, mainly in southeastern Asia,  
647 though the models do differ regarding drought patterns and severity.

648

649 Figure 7 (rightmost column) shows that the link between precipitation over eastern  
650 China, Korea, and Japan with SST varies seasonally, with the strongest ties in DJF and  
651 MAM – reduced precipitation in the region is tied to La Nina and cold Indian Ocean SST.

652 During JJA the correlation to SST is overall weak. During SON the correlations with  
653 precipitation are negative in the western North Pacific and positive in the northern Indian  
654 Ocean and the eastern tropical Pacific.

655

656 These results are consistent with those of Yang and Lau (2004), who found that MAM  
657 precipitation in southeastern China is linked to ENSO – reduced precipitation occurs in  
658 years with an abnormally cold central and eastern tropical Pacific and Indian Ocean.

659 Yang and Lau (2004) found that on average in southern China (south of the Yangtze  
660 River), MAM and JJA precipitation each account for about 35% of the annual total, with  
661 JJA presenting a more complicated picture (see above). They also found that in years  
662 with abnormally warm SSTs over the warm pool and northern Indian Ocean and  
663 abnormally cold SSTs over the western North Pacific, precipitation over central eastern  
664 China tends to be anomalously high (see also Wu et al. [2009, 2010]). They further found  
665 a tendency for a weakened East Asian monsoon circulation and a delayed monsoon onset  
666 in years for which SSTs in the central and eastern tropical Pacific are abnormally warm,  
667 resulting in reduced late summer precipitation over northern China.

668

669 The above linkages are reflected to some extent in the model results of Figure 7 (right  
670 panels), though without any evidence of a strong link to SST in the warm pool. Figure 7  
671 in fact features the typical SST anomaly patterns that dominate the East Asian climate  
672 during the mature phase of El Niño (boreal winter) extending into the decaying-year  
673 summer (Wu et al. 2009). This type of interannual monsoon-SST relationship is well  
674 captured by the AMIP simulations of CMIP3 and CMIP5 models (Song and Zhou 2014a).

675

676 A comparison of the observed and model generated changes in Figure 3 indicates that the  
677 reduced precipitation over southeast China over the last three decades is linked to SST.  
678 Figure 9 shows these long-term changes have occurred primarily during spring and fall,  
679 though DJF does show an enhanced probability of extreme dryness (Fig. 10). Figure 11  
680 shows that the warming of the last three decades is associated with an enhanced  
681 probability of extreme warm seasons especially during JJA over northwest China, Korea  
682 and Japan, and over most of East Asia during SON.

683

### 684 *3.7 India*

685 Kanikicharla et al. (2015), in their comprehensive review of monsoon droughts over  
686 India, note that Indian drought is indeed synonymous with monsoon failure and that a  
687 number of historical droughts there have led to severe famines and great human and  
688 economic losses. They use a century-long time series of Indian summer monsoon rainfall  
689 (ISMR) to capture the characteristic spatio-temporal features of deficit monsoons and  
690 their possible driving mechanisms. They particularly discuss the low-frequency  
691 modulation of ISMR and associated drought area extent in India with respect to global  
692 climate phenomena, and they employ a large suite of AMIP-type model simulations to  
693 assess the predictability of Indian drought.

694

695 Some key findings from that paper are:

696

697 -Monsoon failures are linked to preceding winter and spring snow accumulation over the  
698 Himalayas and larger regions of Eurasia and to the occurrence of warm ENSO events in  
699 the Pacific (with the latter link being much stronger).

700

701 -The leading EOF of Indian monsoon rainfall has a very conspicuous resemblance to the  
702 rainfall anomaly pattern associated with major droughts, and that EOF's time series  
703 correlates well with an ENSO-like SST pattern in the Pacific.

704

705 - The low frequency behavior of monsoon rainfall and drought area index goes hand in  
706 hand with the opposite sign of the NIÑO34 index (which captures the ENSO and AMO),  
707 though with a large difference in their evolution in recent decades. This indicates that the  
708 behavior of the Indian monsoon in recent decades cannot be fully explained by known  
709 global teleconnections and that other factors (e.g., Indian Ocean variability, aerosols)  
710 could be influencing its variability on interannual and decadal time scales (e.g.,  
711 Ramanathan et al. 2005; Lau et al. 2006; Gautam 2009).

712

713 - AGCM simulations forced with global and regional SSTs are able to reproduce the low-  
714 frequency variability well, and runs with observed SSTs in the Pacific but with  
715 climatological SSTs elsewhere generally produce the sign of many droughts in the past  
716 century. The simulated rainfall deficits, however, are much smaller than observed

717



718 - More concerted efforts with climate models are needed to anticipate the severity and  
719 geographical extent of droughts. Global warming is probably altering known  
720 teleconnections, complicating our ability to predict Indian drought.

721

722 These findings emphasize the challenges faced in predicting drought over India and  
723 surrounding regions within a changing climate. Figure 1 (top panel) emphasizes the  
724 weak link of annual mean precipitation over southern Asia to global (and in particular  
725 ENSO) SST in recent decades, though it also shows (bottom panel) that temperature  
726 variations in the broader south Asian monsoon region do have strong ties to global SST.  
727 Figure 7 (middle column of panels) highlights the strong seasonality in the simulated link  
728 between precipitation and SST in recent decades, with only MAM showing a substantial  
729 link to ENSO: El Niño (La Niña) is associated with reduced (enhanced) precipitation.  
730 (This link is consistent with observations and robust across the models [Figure B3].)  
731 ENSO may provide important preconditioning of the land (e.g., soil moisture, snow)  
732 during the pre-monsoon months, so that the role played by SST in monsoon droughts,  
733 while important, may be indirect. We note that such effects may be missed by  
734 contemporaneous correlations, as in the present analyses.

735

### 736 *3.8 Australia and the Maritime Continent*

737 As reviewed in Cai et al. (2014), the influence of climate variability and change on  
738 Australia is complex and varies both regionally and seasonally. In particular, they  
739 indicate how the continent is impacted by the Indian Ocean Dipole (IOD), the Southern

740 Annular Mode (SAM), and El Niño-Southern Oscillation (ENSO), and the poleward edge  
741 of the Southern Hemisphere Hadley cell.

742

743 The corresponding correlation map in Figure 1a shows aspects of a negative IOD, La  
744 Niña and a negative PDO. Consistent with the discussion in Cai et al. (2014), the key  
745 SST forcing regions driving Australian precipitation appear to be the tropical Pacific just  
746 west of the dateline and areas in the eastern Indian Ocean just to the north and west of  
747 Australia. This is highlighted in Figure 8 (left panels), with spring (SON) and summer  
748 (DJF) showing the strongest relationship between Australian precipitation and remote  
749 SST. In summer, the pan-Australian rainfall is dominated by contributions from northern  
750 and eastern Australia; as such, dry conditions are associated with both a warm central  
751 tropical Pacific (with weaker correlations extending eastward across the Pacific), i.e., an  
752 El Niño, and a warm Indian Ocean SST (basin-wide warming that usually accompanies  
753 an El Niño). In spring, the contributions to the pan-Australian rainfall come about equally  
754 from northern and southern Australia, and ENSO and the IOD have the highest coherence  
755 to rainfall in those regions. As such, spring appears to have the strongest (spatially most  
756 coherent) link to ENSO, with dry conditions linked to El Niño and a cool anomaly in the  
757 eastern Indian Ocean. (This result is robust across models and observations [Figure B4].)  
758 In contrast, during fall (MAM) and particularly during winter (JJA), the pan-Australian  
759 precipitation comes mostly from southern Australia. The deficit during fall (MAM)  
760 shows the greatest link with cold SST anomalies to the northwest, while the deficit during  
761 winter (JJA) is linked to cold SST anomalies in the eastern Indian Ocean associated with

762 the development phase of a positive IOD. These cold SST anomalies are unfavorable for  
763 weather systems that typically deliver rain-producing moisture over southern Australia.  
764

765 Recently, Australia experienced one of its most severe droughts ever recorded: the  
766 “Millennium Drought”, which lasted about 10 years (2000-2009). Cai et al. (2014)  
767 showed that the associated precipitation anomalies had substantial seasonal variation,  
768 with austral summer (DJFM) showing positive precipitation anomalies in northwest  
769 Australia and with some of the largest deficits over other parts of Australia occurring  
770 during late fall and winter. Figure 3 shows that the annual mean differences (1998-2011  
771 minus 1979-1993) largely reflect the summer precipitation increases in northwest  
772 Australia during that drought. The relevant seasonality is well captured by the models  
773 (Figure 9), which show the northern Australian precipitation surfeits in the recent 15-year  
774 period during DJFM and the deficits associated with the Millennium Drought during  
775 AMJJ (cf. Figure 3 of Cai et al. [2014]). Much of Australia in fact experienced an  
776 increased risk of dry winters (JJA) over the last fifteen years (Fig. 10).  
777

778 Cai et al. (2014) show that the precipitation deficits over southwest Western Australia  
779 partly result from a long-term upward trend in the Southern Annual Mode (SAM); this  
780 trend accounts for half of the winter rainfall reduction there. For southeast Australia,  
781 CMIP5 model simulations indicate only weak trends in the pertinent climate modes,  
782 apparently underestimating the observed poleward expansion of the subtropical dry-zone  
783 and associated impacts. They conclude that “*although climate models generally suggest*  
784 *that Australia’s Millennium drought was mostly due to multi-decadal variability, some*

785 *late-twentieth-century changes in climate modes that influence regional rainfall are*  
786 *partially attributable to anthropogenic greenhouse warming.”*

787

788 The Maritime Continent is strongly affected by ENSO during JJA and SON (Figure 8,  
789 right panels); El Niño conditions lead to reduced precipitation. JJA also exhibits positive  
790 correlations with tropical and North Atlantic SST. In contrast, DJF and MAM  
791 precipitation show little connection with ENSO, and the overall correlations with SST are  
792 weak – weak negative correlations with SST in the central tropical Pacific, and, for  
793 MAM, weak positive correlations with local SST. Chang et al. (2003), however, point  
794 out that the low correlations between Indonesian rainfall and ENSO during the Northern  
795 Hemisphere winter monsoon period are partly due to the spatial averaging of the rainfall  
796 in two regions with opposite characteristics.

797

### 798 *3.9 Europe and the Mediterranean*

799 Here we review the primary modes of variability that affect European and Mediterranean  
800 climate on subseasonal to interannual and longer time scales, with a focus on their  
801 impacts on precipitation and/or surface temperature fields. We shall see that northern and  
802 central European meteorological drought drivers and impacts are often different or even  
803 opposite to those for southern Europe and the Mediterranean region<sup>9</sup>. In addition, we will  
804 discuss reported trends in meteorological drought in Europe and projected drought  
805 changes in Europe with increasing greenhouse gases.

806

---

<sup>9</sup> In this section, the term Mediterranean is used to indicate areas surrounding the sea from southern Europe, northern Africa and the Middle East; the term Europe indicates northern and central Europe.

807 Correlations of the North Atlantic Oscillation (NAO) and the Atlantic Multidecadal  
808 Oscillation (AMO) with drought occurrence in Europe have been documented, and the  
809 effects of other modes of variability including ENSO have been postulated (see below).  
810 Nonetheless, these relationships do not seem to be associated with high interannual  
811 predictability of meteorological drought in central and northern Europe (Dutra et al.  
812 2014). Overall SST anomalies, which may be associated with large-scale modes of  
813 variability, explain only a small fraction of annual mean variability in precipitation (less  
814 than 10%) and temperature (less than 20%) over Europe (see Fig. 1). Hence the  
815 predictability associated with large-scale modes of variability that have been linked to  
816 drought occurrence in Europe is still unclear from the existing literature. In addition, it  
817 has been highlighted that the circulation patterns and weather types related to the most  
818 severe droughts in Europe often vary across seasons and regions (Stahl 2001, see also  
819 below; Fleig et al. 2011).

820

821 Hurrell (1995) showed that during high NAO index winters (such as those that occurred  
822 in 1983, 1989 and 1990), the axis of maximum moisture transport shifts to a more  
823 southwest-to-northeast orientation across the Atlantic and extends much farther north and  
824 east onto northern Europe and Scandinavia, accompanied by a reduction in moisture  
825 transport over southern Europe, the Mediterranean and northern Africa. As a result,  
826 northern Europe is mild and wet during the positive phase of the NAO and cold and dry  
827 during the negative phase, whereas the reverse is true for southern Europe and most of  
828 the Mediterranean but with the Levant also being wet (dry) during a positive (negative)  
829 NAO (e.g. Xoplaki et al. 2004). In recent decades the NAO index has shown a return

830 toward more negative values, though with marked increase in year-to-year winter  
831 variability (Hanna et al. 2015).

832

833 The summer NAO (sNAO) has a more northerly location and smaller spatial scale than  
834 its winter counterpart (Folland et al. 2009). Nevertheless, the sNAO has a strong  
835 influence on northern European rainfall, temperature, and cloudiness through changes in  
836 the position of the North Atlantic storm track, thus playing an important role in  
837 generating summer climate extremes, including flooding, drought, and heat waves in  
838 northwestern Europe. A positive sNAO also results in wetter conditions in the  
839 central/eastern part of the Mediterranean.

840

841 Folland et al. (2009) further suggest that on interdecadal time scales, sNAO variations are  
842 partly related to the Atlantic Multidecadal Oscillation (AMO). While the exact link  
843 between the two is still unclear, Sutton and Dong (2012) show that, during the 1990s,  
844 European climate shifted towards a pattern characterized by anomalously wet summers in  
845 northern Europe and hot, dry, summers in southern Europe, with related shifts in spring  
846 and autumn, and they point to recent evidence suggesting that the warming was largely  
847 caused by an acceleration of the Atlantic Meridional Overturning Circulation (AMOC)  
848 and associated northward ocean heat transport in response to the persistent positive phase  
849 of the winter NAO in the 1980s and early 1990s (Robson et al. 2012). However,  
850 uncertainties still exist regarding the processes underpinning AMO variability, for  
851 example the role of anthropogenic aerosols (Booth et al. 2012). Mariotti and dell'Aquila  
852 (2012) show that decadal variability associated with the NAO, the sNAO, and the AMO

853 significantly contribute to decadal climate anomalies over the Mediterranean region. The  
854 positive phase of the AMO is associated with warmer than usual decades especially in  
855 summer, whereas the AMO has no influence on Mediterranean winter temperatures.  
856 Land-atmosphere feedbacks also play role in shaping observed decadal variability,  
857 enhancing the large-scale influences. Della Marta et al. (2007) found a relationship  
858 between western Mediterranean heat waves and the AMO. On decadal timescales, the  
859 AMO and NAO explain over 60% of observed area-averaged summer temperature and  
860 winter precipitation variability, respectively (Mariotti and Dell'Aquila, 2012).

861

862 The Mediterranean is one of the main regions worldwide displaying a robust drying trend  
863 in both precipitation and the land water balance since the 1950s (Sheffield et al. 2012;  
864 Hartmann et al. 2013; Greve et al. 2014), a signal consistent with climate change  
865 projections (see below). Nonetheless, a possible attribution of these historical trends to  
866 increased greenhouse gas concentrations has not been provided so far, and it is possible  
867 that decadal variability associated with large-scale modes of variability could have played  
868 a role. Hoerling et al. (2012) note that for the land area surrounding the Mediterranean  
869 Sea, 10 of the 12 driest winters since 1902 occurred in just the last 20 years, and they  
870 propose that the drying over the last century can be understood as a response to a uniform  
871 global ocean warming and to modest changes in the oceans' zonal and meridional SST  
872 gradients, with warming in the Indian Ocean producing an enhanced drying signal  
873 attributable to an atmospheric circulation response resembling the positive phase of the  
874 NAO. Kelley et al. (2011), in a combined observational and modeling analysis, argue  
875 that while the upward NAO-trend over recent decades can explain much of the

876 concurrent Mediterranean region drying, it cannot explain drying in the Levant which  
877 they instead argued was consistent with drying in response to rising greenhouse gases.  
878

879 With respect to climate change projections, the Mediterranean shows one of the most  
880 robust responses (across models) to greenhouse gas increases over the 21<sup>st</sup> Century  
881 (Giorgi and Lionello 2008; Seneviratne et al. 2012; Orłowsky and Seneviratne 2013).  
882 Projected changes, which reinforce trends already observed during the 20<sup>th</sup> Century,  
883 include both a reduction in precipitation and an increase in evapotranspiration (due to  
884 increased incoming radiation and higher air temperature), with associated soil moisture  
885 reductions (e.g. Mariotti et al. 2008; Orłowsky and Seneviratne 2012, 2013; Seager et al.  
886 2014b; Mariotti et al. 2015).

887

888 Uncertainties remain in our understanding of the NAO's link to SST changes (Bretherton  
889 and Battisti 2000) and of its link to global warming (Gillett et al. 2003), its connection  
890 to the Arctic Oscillation (AO, Ambaum et al. 2001), its link to the stratosphere (Scaife  
891 et al. 2005), and its possible modulation by ENSO (Bronnimann 2007) and other modes  
892 of variability such as the Scandinavian (SCA) and the East Atlantic (EA) patterns (e.g.,  
893 Comas-Bru and McDermott 2014). In fact, the SCA, the EA, and the East  
894 Atlantic/western Russia (EAWR) patterns (Barnston and Livezey 1987) have also been  
895 suggested to contribute substantially to European climate variability (e.g. Bueh and  
896 Nakamura 2007; Iglesias et al. 2014; Ionita 2014).

897



898 A number of studies have produced objectively-defined drought catalogues for  
899 Europe (Lloyd-Hughes et al. 2010; Spinoni et al. 2015). Parry et al. (2010) also  
900 produced summaries of the major large-scale European droughts of the last 50 years  
901 based on the catalogue from Lloyd-Hughes et al. (2010). As summarized in Stahl  
902 (2001), major droughts over the period 1960-1990 occurred during 1962-64, 1972-76,  
903 1983, 1989-1990. They note that “*Most of the severe summer droughts across Europe*  
904 *were associated with high pressure systems across central Europe. Generally, drought*  
905 *associated synoptic meteorology is characterised by high MSLP, but the circulation*  
906 *pattern types vary not only with the season but also for all individual discussed events.*”

907  
908 Figures 2b and 11 show that there has been a pronounced shift in the probability of  
909 extremely warm years over the last three decades over most of Europe, with the shift  
910 equal to more than 1.5 times the climatological probability of 2.5% over many regions.  
911 This shift, most pronounced during fall, appears to be associated with a shift in the mean  
912 temperature over the recent decades, which is likely attributable in part to enhanced  
913 greenhouse gas forcing (Bindoff et al. 2013). Figures 2a and 10 show that changes in  
914 precipitation over the last three decades are generally small, though there is a general  
915 tendency for a greater probability of extremely dry years throughout central and southern  
916 Europe. This appears to hold for each season as well. This result is also robust when  
917 investigating longer-term trends since the 1950s, either for precipitation or precipitation  
918 minus evapotranspiration (Seneviratne et al. 2012a; Hartmann et al. 2013; Greve et al.  
919 2014).

920

921 While the present review and special issue focus on meteorological (i.e. precipitation-  
922 based) drought and its relation to SSTs as driver, we note the following additional points  
923 regarding drought drivers in Europe:

924

925 - In general, agricultural (soil moisture) and hydrological (streamflow) drought events in  
926 Europe are caused by a prolonged deficit in precipitation (Tallaksen et al. 2015, Stagge  
927 et al. 2015). However, in Central Europe, evapotranspiration is an important driver for  
928 soil moisture droughts, in some cases to the same degree as precipitation (e.g.  
929 Seneviratne et al. 2012b, Teuling et al. 2013). In addition, in cold climates, temperature  
930 anomalies also play a role in the development of hydrological drought (Van Loon and  
931 Van Lanen 2012).

932

933 - Prior storage deficits in the form of soil moisture, snow and groundwater are important  
934 for the occurrence and development of soil moisture and streamflow droughts (van Loon  
935 and van Lanen 2012, Orth and Seneviratne 2013, Staudinger et al. 2014, Tallaksen et al.  
936 2015). They thus provide some essential sources of drought predictability, in particular  
937 given the low SST control on interannual precipitation variability in Europe (Fig. 1)..

938

### 939 *3.10 Northern Eurasia*

940 Figure 1 shows that across the vast expanse of Northern Eurasia, neither precipitation nor  
941 temperature is strongly affected by SST on interannual time scales. Schubert et al.  
942 (2014), in examining both heat waves and drought over northern Eurasia, highlighted the  
943 central role of anticyclones in the region; these act to warm and dry the atmosphere and

944 land surface over many important agricultural regions from European Russia to  
945 Kazakhstan and beyond. They discuss how the development of anticyclones is linked to  
946 different air masses, especially the intrusion of Arctic air masses that occasionally  
947 combine with subtropical air (e.g., associated with the Azores high in eastern Europe and  
948 western Russia) to produce especially severe drought and heat wave events. Schubert et  
949 al. (2014) found that some of the most severe summer heat waves are linked to distinct  
950 Rossby wave trains spanning the continent that, while producing severe heat in one  
951 location, cause a juxtaposition of wet and cool conditions in regions thousands of miles to  
952 the east or west – a phenomenon noted more than one hundred years ago in early  
953 descriptions of Northern Eurasian heat waves.

954

955 Given the lack of a strong SST connection, the predictability of the most severe events in  
956 Northern Eurasia is limited to the time scales of the internally forced Rossby waves  
957 (typically less than one month), though some aspects of heat waves appear to be  
958 predictable for several months: the surface temperature anomalies at the center of the heat  
959 wave associated with soil moisture anomalies that persist through the summer. Schubert  
960 et al. (2014), using an AGCM experiment in which soil moisture feedbacks were  
961 disabled, showed that temperature variability is strongly tied to soil moisture variability  
962 particularly in the southern parts of Northern Eurasia extending from southern Europe  
963 eastward across the Caucasus, Kazakhstan, Mongolia, and northern China. They note  
964 that longer-term droughts (lasting multiple years) do occur but are largely confined to the  
965 southern parts of Northern Eurasia, where there appears to be a weak link to SST and an  
966 important control from soil moisture.

967

968 Schubert et al. (2014) further showed that the observed warming over northern Eurasia in  
969 the last three decades is part of a large-scale warming pattern with local maxima over  
970 European Russia and over Mongolia/eastern Siberia (see also Fig. 3). Precipitation  
971 changes consist of deficits across Eurasia covering parts of northeastern Europe,  
972 European Russia, Kazakhstan, southeastern Siberia, Mongolia, and northern China and  
973 increases across Siberia poleward of about 60°N. Comparisons of these changes with  
974 Figure 3, however, indicate some sensitivity of the computed changes to the years chosen  
975 for averaging. Model simulations carried out with idealized versions of the observed SST  
976 anomalies indicate that the changes over the last three decades are consistent with a  
977 global-scale response to PDO-like and AMO-like SST patterns, intensified by a global  
978 warming SST trend.

979

980 Figure 2 indicates that any changes in probability of heat waves are likely a consequence  
981 of an overall warming trend that affects much of Eurasia (though more strongly in the  
982 southern regions). In particular, the increase in the probability of extreme heat largely  
983 results from an overall shift in the pdf of temperature (a change in the mean) rather than  
984 from any change in the shape of that pdf. Schubert et al. (2014) point to studies  
985 indicating an enhanced probability of heat waves across northern Eurasia by the second  
986 half of the 21<sup>st</sup> Century. Existing studies and analyses of climate change projections of  
987 the Coupled Model Intercomparison Project (CMIP), however, show less certainty  
988 regarding future drought (e.g. Seneviratne et al. 2012; Orłowsky and Seneviratne 2013),  
989 reflecting the greater uncertainty of precipitation and soil moisture projections.

990

991 **4. Concluding Remarks**

992 The results presented here, and in the regionally-focused articles that make up this special  
993 collection, illustrate that considerable progress has been made in our understanding of the  
994 occurrence and predictability of meteorological drought in different parts of the world.

995 The importance of large-scale teleconnections, whether they are linked to ENSO or other  
996 SST variability or whether they consist of large-scale atmospheric circulation anomalies  
997 that are unforced by SST (internal to the atmosphere), is now well established. As such,  
998 in addressing the causes and predictability of meteorological drought for any particular  
999 region of the world, we have to address the following questions: 1) what are the large-  
1000 scale drivers (if any) of precipitation deficits relevant to that region, and 2) what are the  
1001 unique climatological features of that region that act to enhance or suppress the large  
1002 scale precipitation tendencies.

1003

1004 Although the individual articles have in many cases provided answers to both of these  
1005 questions and we have attempted to summarize them in Section 3, this article goes further  
1006 by providing a more global perspective on these two questions in the context of the  
1007 “consensus” view provided by the simulations with current state-of-the-art AGCMs  
1008 forced by observed SST.

1009

1010 In particular, we have provided our current best estimate of where SST forcing provides  
1011 some control on annual precipitation and temperature variability. This is critically  
1012 important to the drought prediction problem, since the regions where SST do play a

1013 substantial role in driving precipitation (and temperature) variability, are also the regions  
1014 where we can expect to have some degree of predictability on seasonal and longer time  
1015 scales. We have also underscored the importance of ENSO (tropical Pacific SST) in  
1016 providing that potential predictability in many parts of the world (including the Americas,  
1017 eastern and southwest Asia, Australia and the Maritime Continent) though not  
1018 exclusively so, with other Ocean basins also playing a role in some regions of the world,  
1019 either individually or in concert with ENSO. These include the Indian Ocean (the Indian  
1020 Ocean dipole affecting Australia, the Indian Ocean basin mode affecting East Asia), the  
1021 Atlantic Ocean (affecting northern South America, parts of the southern and eastern US,  
1022 and the Sahel), and the Mediterranean Sea (affecting southern Europe and northern  
1023 Africa), though the extent to which some of these SST patterns are independent of ENSO  
1024 is still not fully resolved.

1025

1026 A number of regions dominated by monsoonal climates have droughts that are intimately  
1027 tied to failures in the development of monsoonal rains. The GDIS papers highlight the  
1028 substantial progress made in identifying the sources of these failures. From a global  
1029 perspective, ENSO significantly affects much of the Asian-Australian monsoon system.  
1030 On decadal time scales, the apparent weakening of the global land monsoon since the  
1031 1950s has been linked to the Inter-decadal Pacific Oscillation as well as to a warming  
1032 trend over the central-eastern Pacific and the western tropical Indian Ocean. Much  
1033 remains to be understood, however, about the observed trends in monsoonal precipitation.

1034

1035 Northern Eurasia, central Europe, and central and eastern Canada stand out as regions  
1036 with little SST-forced impacts on precipitation on interannual time scales. This has  
1037 important implications for the predictability and the time scales of droughts in these  
1038 regions. In Northern Eurasia, for example, droughts and heat waves are predominantly  
1039 linked to the development of anticyclones, and although extreme, they rarely last longer  
1040 than one season. In central Europe a number of different atmospheric teleconnections  
1041 that are unforced (or only weakly forced) by SST do appear to play a role, though these  
1042 are relatively short lived and have little predictability on seasonal and longer time scales:  
1043 here evapotranspiration is an important driver for soil moisture droughts, and  
1044 predictability on longer time scales is tied to soil moisture memory and feedbacks.

1045

1046 Although the annual mean results provide a broad picture of the role of SST, our results  
1047 also highlight the strong seasonality in the link to the SST that occurs in most regions of  
1048 the world. As such, the timing and duration of drought has as much to do with the  
1049 seasonality of the link to SST, as it has to do with the time of year that local  
1050 climatological (land, circulation) conditions make a region most prone to drought. East  
1051 Africa is an example of a particularly challenging region for which to model and  
1052 understand drought, due to heterogeneous local rainfall regimes that include unimodal  
1053 and bimodal annual cycles combined with strong seasonality in the response to ENSO.

1054

1055 We have also addressed longer-term (decadal) meteorological drought and the link to  
1056 SST. In particular, we present a remarkable example of the ability of current climate  
1057 models (when forced with observed SST) to reproduce the long-term changes in

1058 precipitation and surface temperature that have occurred over the last three decades. The  
1059 model results show that the shifts to drought or pluvial conditions (and warming) have a  
1060 global coherence driven by long-term SST changes (a combination of the PDO, AMO,  
1061 and a long term trend). Our analysis of the most extreme seasonal and annual mean  
1062 precipitation deficits shows that the associated changes in the tails of the probability  
1063 density functions (PDFs) in most regions of the world reflect the overall shifts in the  
1064 mean rather than changes in the shape of the PDFs (though this may not be true for  
1065 northeastern South America – a region exhibiting a substantial decrease in the probability  
1066 of extremely dry years over the last three decades though with little change in the  
1067 probability of extreme wet years). The success of the models in reproducing the  
1068 observed changes provides the basis for further research to dissect the causes of these  
1069 changes and address their potential predictability.

1070

1071 One consequence of the decadal and longer-term variations is that a number of regions  
1072 exhibit substantial non-stationarity in the relationships between SST and precipitation on  
1073 interannual time scales (examples where this is particularly evident include west Africa  
1074 and India), complicating our ability to understand these relationships, and take advantage  
1075 of them for prediction. Global warming, while not a focus of this paper, is clearly an  
1076 important issue when addressing longer-term changes in drought. In fact, as discussed in  
1077 a number of the contributed papers, some regions of the world appear to already be  
1078 seeing the impacts of warming on drought (e.g., the southwestern U.S., the Mediterranean  
1079 region and central Europe), though much work needs to be done to better understand the  
1080 relative contributions of decadal SST variability and long term SST trends to drought.



1081

1082 Finally, we must emphasize that current climate models, including the AGCMs used  
1083 here, are far from perfect. A key factor emphasized in many of the contributing papers  
1084 and further highlighted here is the challenge of reproducing some of the complex local  
1085 precipitation regimes (including the annual cycle) that must be simulated correctly in  
1086 order to properly simulate the impact of large scale forcing on regional drought. The  
1087 relatively coarse resolution of current climate models hinders that, and so we can at best  
1088 obtain a spatially averaged picture or in some cases even an incorrect assessment of the  
1089 impacts. Examples where this is especially critical include East Africa and East Asia –  
1090 regions that are characterized by complex terrain and highly heterogeneous regional  
1091 precipitation regimes. We should note that this situation will likely improve in the  
1092 coming years as it becomes feasible to apply ultra-high resolution (sub 10 km) global  
1093 models to climate problems. However, not all problems concerning the simulation of  
1094 important teleconnections can be blamed on insufficient resolution. For example,  
1095 deficiencies in the simulation of the atmospheric response to equatorial Atlantic SSTs and  
1096 the link to west African drought are likely tied to deficiencies in the simulation of the  
1097 climatological mean state. Furthermore, considerable work still needs to be done to  
1098 improve our coupled atmosphere-ocean general circulation models that still have, for  
1099 example, great difficulties in correctly reproducing the seasonal cycle and variability of  
1100 tropical Atlantic SST.

1101

1102 How do we move forward? Drought is an immensely complex problem that must be  
1103 attacked on many fronts by researchers from around the world, with well-considered

1104 links to users who may benefit from the research. GDIS is an ongoing activity that  
1105 supports this cause. GDIS will continue to encourage researchers and users around the  
1106 world to work together to improve systematically our understanding of, prediction of, and  
1107 adaptation to drought, e.g., by facilitating the development of improved models and long  
1108 term consistent drought-specific observations, and providing global access to data portals  
1109 that summarize our ever-evolving knowledge on the subject.

1110

1111 *Acknowledgements:* The various contributions to this paper were made possible by the  
1112 support of the host organizations of the co-authors, as noted in the acknowledgments of  
1113 the contributing Global Drought Information System (GDIS) special collection papers.  
1114 The GDIS effort is sponsored and supported by the World Climate Research Program  
1115 (WCRP: CLIVAR and GEWEX) and various partner organizations including the US  
1116 National Oceanic and Atmospheric Administration (NOAA), the US National  
1117 Aeronautics and Space Administration (NASA), the US National Integrated Drought  
1118 Information System (NIDIS), the World Meteorological Organization (WMO), the US  
1119 CLIVAR program, the Group on Earth Observations (GEO), the European  
1120 Commission Joint Research Centre (JRC), the National Science Foundation (NSF),  
1121 and the European Space Agency (ESA)-European Space Research Institute  
1122 (ESRIN). Support for the overall development of this synthesis paper was provided by  
1123 NASA's Modeling, Analysis and Prediction Program. The GLDAS-2 data used in this  
1124 study were acquired as part of the mission of NASA's Earth Science Division and  
1125 archived and distributed by the Goddard Earth Sciences (GES) Data and Information  
1126 Services Center (DISC).

1127

1128

1129 **Appendix A: Description of the Models and Experiments**

1130 Many of the results presented in this paper are based on Atmospheric Model  
1131 Intercomparison Project (AMIP)-style simulations produced with 5 different Atmospheric  
1132 General Circulation Models (AGCMs). The models used are GEOS-5, CCM3, CAM4,  
1133 GFS, and ECHAM5. *The years 1979-2011 were subsetted from 12 of each model's*  
1134 *ensemble members, providing a dataset of 60 33-yr simulations.* The following provides  
1135 a brief description of the models and the experiments.

1136

1137 The NASA Goddard Earth Observing System Model, Version 5 (GEOS-5) Atmospheric  
1138 General Circulation model (AGCM) is described by Rienecker et al. (2008), and an  
1139 overview of the model's performance is provided by Molod et al. (2012). For these  
1140 experiments, the model was run with 72 hybrid-sigma vertical levels extending to  
1141 0.01hPa and with a 1° horizontal resolution on a latitude/longitude grid. The simulations  
1142 consist of twelve ensemble members, each forced with observed monthly SST, sea ice,  
1143 and time-varying greenhouse gases for the period 1871-present. See Schubert et al.  
1144 (2014) for further details.

1145

1146 A 16-member ensemble covering the period January 1856 to April 2014 was produced  
1147 with the NCAR Community Climate Model 3 (CCM3, Kiehl et al. (1998)). The model  
1148 was run at T42 resolution with 18 vertical levels. Sea ice was held at climatological  
1149 values, and SST forcing in the years of interest here combined the Kaplan et al. (1998)  
1150 SST dataset in the tropical Pacific Ocean (20°N to 20°S) with the Hadley Centre dataset  
1151 (Rayner et al. 2003) outside of the tropical Pacific.

1152

1153 A 20-member ensemble covering the period January 1979 to April 2014 was produced  
1154 with the NCAR Community Atmosphere Model 4 (CAM4), forced by SST and sea ice  
1155 from the Hurrell et al. (2008) data set and with time varying GHGs from the RCP6.0  
1156 scenario after 2005. The resolution used was  $0.94^{\circ} \times 1.25^{\circ}$ , with 26 vertical levels.

1157

1158 The NOAA Earth System Research Laboratory produced a 50-member ensemble  
1159 spanning January 1979 to April 2014 using the NCEP Global Forecast System (GFS, the  
1160 atmosphere component of the Coupled Forecast System) version 2 model denoted here as  
1161 (ESRL GFSv2). The model was run at T126 resolution with 64 vertical levels and was  
1162 forced by observed SST and sea ice from the Hurrell et al. (2008) data. CO<sub>2</sub> varied with  
1163 time, but other GHGs were held fixed.

1164

1165 A 20-member ensemble spanning January 1979 through April 2014 was produced with  
1166 the ECHAM5 model (Roeckner et al. 2003) forced by the Hurrell et al. (2008) SST and  
1167 sea ice data, as recommended for use in CMIP5 simulations. These simulations used  
1168 time-varying GHGs, following the RCP6.0 scenario after 2005, and they used a T159  
1169 resolution, with 31 vertical levels.

1170

1171

1172 **Appendix B: Selected Individual Model Results**

1173 Here we present a few comparisons of the results for individual models and observations,  
1174 highlighting regions where it is especially important to assess the model-dependence of  
1175 the results (see main text). While the comparison with observations provides a rough  
1176 idea of consistency with nature, it must be kept in mind that the observations represent a  
1177 single realization of nature and thus should differ from the ensemble means of the model  
1178 runs, which specifically isolate the impact of SST and other forcings – our focus here. A  
1179 careful assessment of the veracity of the models, which is beyond the scope of this paper,  
1180 would in principle involve determining if a correlation produced for the observations lies  
1181 within the spread produced by the given model’s individual ensemble members.

1182

1183 *(Figure B1 here)*

1184 *(Figure B2 here)*

1185 *(Figure B3 here)*

1186 *(Figure B4 here)*

1187 *(Figure B5 here)*

1188

1189 **References**

1190 Ambaum, M. H. P., B. J. Hoskins, and D. B. Stephenson, 2001: Arctic Oscillation or  
1191 North Atlantic Oscillation? *J. Climate*, **14**, 3495–3507.

1192 doi: [http://dx.doi.org/10.1175/1520-0442\(2001\)014<3495:AOONAO>2.0.CO;2](http://dx.doi.org/10.1175/1520-0442(2001)014<3495:AOONAO>2.0.CO;2)

1193

1194 Barlow, M., B. Zaitchik, S. Paz, E. Black, J. Evans, A. Hoell, 2015: A Review of  
1195 Drought in the Middle East and Southwest Asia. *J. Climate*. Under review.

1196

1197 Barnston A.G., Livezey R.E., 1987: Classification, seasonality and persistence of low-  
1198 frequency atmospheric circulation patterns. *Mon. Wea. Rev.*, **115**, 1083–1126.

1199

1200 Barreiro, M., N. Diaz, 2011: Land-atmosphere coupling in El Niño influence over South  
1201 America. *Atmos. Sci. Lett.*, **12**, 351-355, doi: 10.1002/asl.348.

1202

1203 Bindoff, N.L., P.A. Stott, K.M. AchutaRao, M.R. Allen, N. Gillett, D. Gutzler, K.

1204 Hansingo, G. Hegerl, Y. Hu, S. Jain, I.I. Mokhov, J. Overland, J. Perlwitz, R. Sebbari and

1205 X. Zhang, 2013: Detection and Attribution of Climate Change: from Global to Regional.

1206 In: *Climate Change 2013: The Physical Science Basis. Contribution of Working Group*

1207 *I to the Fifth Assessment Report of the Intergovernmental Panel on Climate Change*

1208 [Stocker, T.F., D. Qin, G.-K. Plattner, M. Tignor, S.K. Allen, J. Boschung, A. Nauels, Y.

1209 Xia, V. Bex and P.M. Midgley (eds.)]. Cambridge University Press, Cambridge, United

1210 Kingdom and New York, NY, USA.

1211

1212 Booth, B. B. B., N. J. Dunstone, P. R. Halloran, T. Andrews, and N. Bellouin, 2012:  
1213 Aerosols implicated as a prime driver of twentieth-century North Atlantic climate  
1214 variability. *Nature*, 484, 228–232.  
1215

1216 Bretherton, C. S. and D. S. Battisti, 2000: An interpretation of the results from  
1217 atmospheric general circulation models forced by the time history of the observed sea  
1218 surface temperature distribution. *Geophys. Res. Lett.*, 27, 767-770.  
1219

1220 Brönnimann, S., 2007: Impact of El Niño-Southern Oscillation on European climate.  
1221 *Rev. Geophys.* 45, RG3003, doi: 10.1029/2006RG000199.  
1222

1223 Bueh C. and H. Nakamura, 2007: Scandinavian pattern and its climatic impact. *Q. J. R.*  
1224 *Meteorol. Soc.* 133 2117–31.  
1225

1226 Cai, W., A. Purich, T. Cowan, P. van Rensch, E. Weller, 2014: Did Climate Change-  
1227 Induced Rainfall Trends Contribute to the Australian Millennium Drought? *J. Climate*,  
1228 27, 3145 – 3168.  
1229

1230 Cazes-Boezio, G., A. W. Robertson, and C. R. Mechoso, 2003: Seasonal dependence of  
1231 ENSO teleconnections over South America and relationships with precipitation in  
1232 Uruguay. *J. Climate*, 16, 1159–1176.  
1233



1234 Chang, P., R. Saravanan, and L. Ji, 2003: Tropical Atlantic seasonal predictability: The  
1235 roles of El Niño remote influence and thermodynamic air–sea feedback. *Geophys. Res.*  
1236 *Lett.*,30,1501, doi:10.1029/2002GL016119.

1237

1238 Chen, H., T. Zhou, R. B. Neale, X. Wu, G. Zhang, 2010: Performance of the New NCAR  
1239 CAM3.5 in East Asian Summer Monsoon Simulations: Sensitivity to Modifications of  
1240 the Convection Scheme. *J. Climate*, 23, 3657-3675.

1241

1242 Comas-Bru, L. and F. McDermott, 2014: Impacts of the EA and SCA patterns on the  
1243 European twentieth century NAO–winter climate relationship. *Q. J. R. Meteorol. Soc.*,  
1244 140, 354–363, January 2014B.

1245

1246 Cook, B.I., T.R. Ault, and J.E. Smerdon, 2015: Unprecedented 21st-century drought risk  
1247 in the American Southwest and Central Plains. *Sci. Adv.*, 1, no. 1, e1400082,  
1248 doi:10.1126/sciadv.1400082.

1249

1250 Dai, A., K. E. Trenberth, and T. Qian, 2004: A global data set of Palmer Drought  
1251 Severity Index for 1870-2002: Relationship with soil moisture and effects of surface  
1252 warming. *J. Hydrometeorology*, 5, 1117-1130.

1253

1254 Della-Marta, P. M., J. Luterbacher, H. von Weissenfluh, E. Xoplaki, M. Brunet, H.  
1255 Wanner, 2007: Summer heat waves over western Europe 1880-2003, their relationship to  
1256 large-scale forcings and predictability. *Clim. Dyn.*, 29, 251-275. DOI 10.1007/s00382-

1257 007-0233-1.  
1258  
1259 Diaz, A. F., C. D. Studzinski and C. R. Mechoso, 1997: Relationships between  
1260 precipitation anomalies in Uruguay and southern Brazil and sea surface temperature in  
1261 the Pacific and Atlantic oceans. *J. Climate*, 11, 251-271.  
1262  
1263 Ding, Q., and B. Wang, J. M. Wallace, and G. Branstator, 2011: Tropical–extratropical  
1264 teleconnections in boreal summer: Observed interannual variability. *J. Climate*, 24,  
1265 1878–1896, doi: 10.1175/2011JCLI3621.1.  
1266  
1267 Dutra et al., 2014: Global meteorological drought – Part 2: Seasonal forecasts. *Hydrol.*  
1268 *Earth Syst. Sci.*, 18, 2669-2678.  
1269  
1270 Fleig, A.K., L.M. Tallaksen, H. Hisdal, and D.M. Hannah, 2011: Regional hydrological  
1271 drought in north-western Europe: Linking a new Regional Drought Area Index with  
1272 weather types. *Hydrological Processes*, 25, 1163–1179.  
1273  
1274 Folland, C. K., Colman, A. W., Rowell, D. P. and Davey, M. K. 2001. Predictability of  
1275 northeast Brazil rainfall and real-time forecast skill, 1987–98. *J. Climate*, 14, 1937–1958.  
1276  
1277 Folland, Chris K., Jeff Knight, Hans W. Linderholm, David Fereday, Sarah Ineson, and  
1278 James W. Hurrell, 2009: The Summer North Atlantic Oscillation: Past, Present, and  
1279 Future. *J. Climate*, **22**, 1082–1103. doi: <http://dx.doi.org/10.1175/2008JCLI2459.1>

1280

1281 Funk, C., M. D. Dettinger, J. C. Michaelsen, J. P. Verdin, M. E. Brown, M. Barlow, and  
1282 A. Hoell, 2008: Warming of the Indian Ocean threatens eastern and southern African  
1283 food security but could be mitigated by agricultural development. *Proc. Natl. Acad. Sci.*  
1284 USA, **105**, 11081–11086, doi:10.1073/pnas.0708196105.

1285

1286 Gautam, R., [N. C. Hsu](#), [W. Lau](#), and M. Kafatos (2009), Aerosol and rainfall variability  
1287 over the Indian monsoon region: distributions, trends and coupling, *Ann. Geophys.*, *27*,  
1288 3691-3703.

1289

1290 Giannini, A., Saravanan, R. and Chang, P. 2004. The preconditioning role of tropical  
1291 Atlantic variability in the development of the ENSO teleconnection: implications for the  
1292 prediction of Nordeste rainfall. *Clim. Dyn.* *22*, DOI: 10.1007/s00382–004-0420-2, 839–  
1293 855.

1294

1295 Gillett, N. P., F. W. Zwiers, A. J. Weaver, and P. A. Stott, 2003: Detection of human  
1296 influence on sea-level pressure, *Nature*, *422*, 292–294.

1297

1298 Giorgi, F., and P. Lionello, 2008: Climate change projections for the Mediterranean  
1299 region. *Global and Planetary Change*, *63*, 90-104.

1300

1301 Goddard, L., Barnston, A. G. and Mason, S. J. 2003. Evaluation of the IRI's 'net  
1302 assessment' seasonal climate forecasts: 1997–2001. *Bull. Amer. Meteor. Soc.* *84*, 1761–

1303 1781.

1304

1305 Greve, P., B. Orlowsky, B. Mueller, J. Sheffield, M. Reichstein, and S.I. Seneviratne,  
1306 2014: Global assessment of trends in wetting and drying over land. *Nature Geoscience*, 7,  
1307 716-721, doi: 10.1038/NGEO2247.

1308

1309 Hanna, E., T.E. Cropper, P.D. Jones, A.A. Scaife, R. Allan, 2015: Recent seasonal  
1310 asymmetric changes in the NAO (a marked summer decline and increased winter  
1311 variability) and associated changes in the AO and Greenland Blocking Index. *Int. J.*  
1312 *Climatol.*, 35, 2540-2554.

1313

1314 Hartmann, D.L., A.M.G. Klein Tank, M. Rusticucci, L.V. Alexander, S. Br. nnimann, Y.  
1315 Charabi, F.J. Dentener, E.J. Dlugokencky, D.R. Easterling, A. Kaplan, B.J. Soden, P.W.  
1316 Thorne, M. Wild and P.M. Zhai, 2013: Observations: Atmosphere and Surface. In:  
1317 *Climate Change 2013: The Physical Science Basis. Contribution of Working Group*  
1318 *I to the Fifth Assessment Report of the Intergovernmental Panel on Climate Change*  
1319 [Stocker, T.F., D. Qin, G.-K. Plattner, M. Tignor, S.K. Allen, J. Boschung, A. Nauels, Y.  
1320 Xia, V. Bex and P.M. Midgley (eds.)]. Cambridge University Press, Cambridge, United  
1321 Kingdom and New York, NY, USA.

1322

1323 Hartmann, D., 2015: Pacific sea surface temperature and the winter of 2014. *Geophys.*  
1324 *Res. Let.* Doi:10.1002/2015GL063083

1325

1326 Hoell, A., and C. Funk, 2013: The ENSO-related West Pacific sea surface temperature  
1327 gradient. *J. Climate*, 26, 9545-9562, doi:10.1175/JCLI-D-12-00344.1.  
1328  
1329 \_\_\_\_\_, and \_\_\_\_\_, 2014: Indo-Pacific sea surface temperature influences on failed  
1330 consecutive rainy seasons over eastern Africa. *Climate Dyn.*, 43, 1645-1660,  
1331 doi:10.1007/s00382-013-1991-6.  
1332  
1333 Hoerling, M. P., and A. Kumar, 2003: The perfect ocean for drought. *Science*, 299, 691-  
1334 694.  
1335  
1336 Hoerling, Martin, Jon Eischeid, Judith Perlwitz, Xiaowei Quan, Tao Zhang, and Philip  
1337 Pegion, 2012: On the Increased Frequency of Mediterranean Drought. *J. Climate*, 25,  
1338 2146–2161. doi: <http://dx.doi.org/10.1175/JCLI-D-11-00296.1>  
1339  
1340 Hoerling, M., J. Eischeid, A. Kumar, R. Leung, A. Mariotti, K. Mo, S. Schubert, and R.  
1341 Seager, 2014: Causes and Predictability of the 2012 Great Plains Drought. *Bull. Amer.*  
1342 *Meteor. Soc.*, 95, 269–282. doi: <http://dx.doi.org/10.1175/BAMS-D-13-00055.1>  
1343  
1344 Hurrell, J. W., 1995: Decadal trends in the North Atlantic Oscillation: regional  
1345 temperatures and precipitation. *Science*, 269, 676-679.  
1346

1347 Hurrell, James W., James J. Hack, Dennis Shea, Julie M. Caron, and James Rosinski,  
1348 2008: A New Sea Surface Temperature and Sea Ice Boundary Dataset for the Community  
1349 Atmosphere Model. *J. Climate*, 21, 5145–5153.  
1350 doi: <http://dx.doi.org/10.1175/2008JCLI2292.1>  
1351  
1352 Iglesias I., Lorenzo M. N., Taboada J. J., 2014: Seasonal Predictability of the East  
1353 Atlantic Pattern from Sea Surface Temperatures. *PLoS ONE* 9(1): e86439. doi:10.1371/  
1354 journal.pone.0086439  
1355  
1356 Ionita, M., 2014: The Impact of the East Atlantic/Western Russia Pattern on the  
1357 Hydroclimatology of Europe from Mid-Winter to Late Spring. *Climate*, 2(4), 296-309.  
1358 doi:10.3390/cli2040296.  
1359  
1360 IPCC, 2001: *Climate Change 2001: Impacts, Adaptation and Vulnerability*, Contribution  
1361 of Working Group II to the Third Assessment Report of the Intergovernmental Panel on  
1362 Climate Change. [McCarthy, J. J.; Canziani, O. F.; Leary, N. A.; Dokken, D. J.; and  
1363 White, K. S., ed.], Cambridge University Press, ISBN 0-521-80768-9 (pb: 0-521-01500-  
1364 6).  
1365  
1366 IPCC, 2007: *Climate Change 2007: The Physical Science Basis*. Contribution of Working  
1367 Group I to the Fourth Assessment Report of the Intergovernmental Panel on Climate  
1368 Change [Solomon, S., D. Qin, M. Manning, Z. Chen, M. Marquis, K.B. Averyt, M.

1369 Tignor and H.L. Miller (eds.)). Cambridge University Press, Cambridge, United  
1370 Kingdom and New York, NY, USA, 996 pp.  
1371  
1372 IPCC, 2013: Climate Change 2013: The Physical Science Basis. Contribution of Working  
1373 Group I to the Fifth Assessment Report of the Intergovernmental Panel on Climate  
1374 Change [Stocker, T.F., D. Qin, G.-K. Plattner, M. Tignor, S.K. Allen, J. Boschung, A.  
1375 Nauels, Y. Xia, V. Bex and P.M. Midgley (eds.)]. Cambridge University Press,  
1376 Cambridge, United Kingdom and New York, NY, USA, 1535 pp,  
1377 doi:10.1017/CBO9781107415324.  
1378  
1379 Kanikicharla, K. K., A. Kulkarni, S. Pai and S. Nigam, 2015: Monsoon droughts in India,  
1380 J. Climate, under review.  
1381  
1382 Kaplan, A., M. A. Cane, Y. Kushnir, A. C. Clement, M. B. Blumenthal, and B.  
1383 Rajagopalan, 1998: Analyses of global sea surface temperature 1856– 1991. J. Geophys.  
1384 Res., 103, 18,567– 18,589.  
1385  
1386 Kelley, C., M. Ting, R. Seager and Y. Kushnir, 2011: The relative contributions of  
1387 radiative forcing and internal climate variability to the late 20th Century winter drying of  
1388 the Mediterranean region. Clim. Dyn., 38, 2001-2015.  
1389

1390 Kiehl J. T., Hack J. J., Bonan G. B., Boville B. A., Williamson D. L., Rasch P. J., 1998:  
1391 The National Center for Atmospheric Research Community Climate Model: CCM3. J.  
1392 Climate, 11, 113-1149.  
1393  
1394 Kim H. M., P. J. Webster, J. A. Curry and V. E. Toma, 2012: Asian summer monsoon  
1395 prediction in ECMWF System 4 and NCEP CFSv2 retrospective seasonal forecasts.  
1396 Climate Dyn., 39(12), 2975-2991.  
1397  
1398 Koster, R. D. and Coauthors, 2004: Regions of strong coupling between soil moisture and  
1399 precipitation. Science, 305, 1138–1140.  
1400  
1401 Kushnir, Y., R. Seager, M. Ting, N. Naik and J. Nakamura, 2010: Mechanisms of tropical  
1402 Atlantic SST influence on North American precipitation variability. J. Climate, 23, 5610-  
1403 5628.  
1404 Lau, K. M., Kim, M. K., and Kim, K. M., 2006: Asian monsoon anomalies induced by  
1405 aerosol direct effects, Clim. Dynam., 26, 855–864, doi:10.1007/s00382-006-0114-z.  
1406  
1407 Li, H., A. Dai, T. Zhou, J. Lu, 2010: Responses of East Asian summer monsoon to  
1408 historical SST and atmospheric forcing during 1950-2000, Clim. Dyn., 34, 501-514, DOI  
1409 10.1007/s00382-008-0482-7.  
1410



1411 Li, J., R. Yu, W. Yuan, H. Chen, W. Sun, Y. Zhang, 2015: Precipitation over East Asia  
1412 simulated by NCAR CAM5 at different horizontal resolutions. *Journal of Advances in*  
1413 *Modeling Earth Systems*, 7(2), 774-790. DOI 10.1002/2014MS000414.  
1414

1415 Li, S. L., J. Lu, G. Huang, and K. M. Hu, 2008: Tropical Indian Ocean basin warming  
1416 and East Asian summer monsoon: A multiple AGCM study. *J. Climate*, 21, 6080–6088.  
1417

1418 Liebmann, B., M.P. Hoerling, C. Funk, I. Bladé, R.M. Dole, D. Allured, X. Quan, P.  
1419 Pegion, and J.K. Eischeid, 2014: Understanding Recent Eastern Horn of Africa Rainfall  
1420 Variability and Change. *J. Climate*, 27, 8630–8645. doi: <http://dx.doi.org/10.1175/JCLI->  
1421 [D-13-00714.1](http://dx.doi.org/10.1175/JCLI-D-13-00714.1)  
1422

1423 Lloyd-Hughes B., J. Hannaford, S. Parry, C. Keef, C. Prudhomme and H.G. Rees, 2010:  
1424 Drought Catalogues for UK and Europe. Environment Agency Science Report  
1425 SC070079/SR Environment Agency: Bristol.  
1426

1427 Losada, T., B. Rodriguez-Fonseca, E. Mohino, J. Bader, S. Janicot, and C. R. Mechoso, 2012:  
1428 Tropical SST and Sahel rainfall: A non-stationary relationship. *Geophys. Res. Lett.*, 39, L12705,  
1429 doi:[10.1029/ 2012GL052423](https://doi.org/10.1029/2012GL052423).  
1430

1431 Lyon, B. and D.G. DeWitt, 2012: A recent and abrupt decline in the East African long  
1432 rains. *Geophys. Res. Lett.*, 39, L02702, doi: [10.1029/2011GL050337](https://doi.org/10.1029/2011GL050337).  
1433

1434 Lyon, B., A.G. Barnston, and D.G. DeWitt, 2013: Tropical Pacific forcing of a 1998-99  
1435 climate shift: Observational analysis and climate model results for the boreal spring  
1436 season. *Climate Dyn.*, 43, 893-909, doi 10.1007/s00382-013-1891-9.  
1437

1438 Lyon, B., 2014: Seasonal Drought in the Greater Horn of Africa and its Recent Increase  
1439 During the March-May Long Rains. *J. Climate*, 27, 7953-7975.  
1440

1441 Ma, H. -Y., C. R. Mechoso, Y. Xue, H. Xiao, C. -M. Wu, J. -L. Li, and F. De Sales,  
1442 2010: Impact of land surface processes on the South American warm season climate.  
1443 *Clim. Dyn.* doi: 10.1007/s00382-010-0813-3.  
1444

1445 Magaña, Victor, Jorge A. Amador, and Socorro Medina, 1999: The Midsummer Drought  
1446 over Mexico and Central America. *J. Climate*, **12**, 1577–1588.  
1447 doi: [http://dx.doi.org/10.1175/1520-0442\(1999\)012<1577:TMDOMA>2.0.CO;2](http://dx.doi.org/10.1175/1520-0442(1999)012<1577:TMDOMA>2.0.CO;2)  
1448

1449 Marengo, J. A., and Coauthors, 2008: The drought of Amazonia in 2005. *J. Climate*, 21,  
1450 495–516.  
1451

1452 [Marengo, J. A., R. Jones, L. M. Alves and M. C. Valverde, 2009: Future change of](#)  
1453 [temperature and precipitation extremes in South America as derived from the PRECIS](#)  
1454 [regional climate modeling system. \*Int. J. Climatol.\*, 29, 2241-2255.](#)  
1455

1456 Mariotti, A., 2007: How ENSO impacts precipitation in southwest central Asia, *Geophys.*  
1457 *Res. Lett.*, 34, L16706, doi:101029/2007GL030078.

1458

1459 Mariotti A., N. Zeng , J. Yoon, V. Artale, A. Navarra, P. Alpert, and L.Z.X. Li, 2008:  
1460 Mediterranean water cycle changes: transition to drier 21st century conditions in  
1461 observations and CMIP3 simulations. *Environ.. Res. Lett.*, 3, 044001 (8pp),  
1462 doi:10.1088/1748-9326/3/4/044001.

1463

1464 Mariotti, A. and A. Dell'Aquila, 2012: Decadal climate variability in the Mediterranean  
1465 region: roles of large-scale forcings and regional processes, *Clim. Dyn.*, 38, 1129–1145,  
1466 DOI 10.1007/s00382-011-1056-7.

1467

1468 Mariotti A., Y. Pan, N. Zeng, and A. Alessandri, 2015: Long-term climate change in the  
1469 Mediterranean region in the midst of decadal variability. *Climate Dyn.*, 44 (5-6), pp  
1470 1437-1456, doi:10.1007/s00382-015-2487-3.

1471

1472 McCarthy et al. (2001): Climate Change 2001:Working Group II: Impacts, Adaptation  
1473 and Vulnerability. Chapter 14. 14.1.2.1.4. Variability and impacts from El Niño and the  
1474 Southern Oscillation. [McCarthy, J. J.; Canziani, O. F.; Leary, N. A.; Dokken, D. J.; and  
1475 White, K. S., ed.], Cambridge University Press, ISBN 0-521-80768-9 (pb: 0-521-01500-  
1476 6).

1477

1478 Mechoso, C. R., and S. W. Lyons, 1988: On the atmospheric response to SST anomalies  
1479 associated with the Atlantic warm event during 1984. *J. Climate*, 1, 422-428.

1480

1481 Mechoso, C. R., A. Robertson, and coauthors, 1995: The seasonal cycle over the tropical  
1482 Pacific in coupled ocean-atmosphere general circulation models. *Mon. Wea. Rev.*, 123,  
1483 2825–2838.

1484

1485 Mo, K. C., and E. H. Berbery, 2011: Drought and persistent wet spells over South  
1486 America based on observations and the U.S. CLIVAR drought experiments. *J. Climate*,  
1487 24, 1801-1820.

1488

1489 Mohino, E., S. Janicot, and J. Bader, 2011a: Sahelian rainfall and decadal to multidecadal  
1490 SST variability. *Climate Dyn.*, 37, 419–440, doi:[10.1007/s00382-010-0867-2](https://doi.org/10.1007/s00382-010-0867-2).

1491

1492 Mohino,E., Belén Rodríguez-Fonseca, Teresa Losada, Sébastien Gervois, Serge Janicot,  
1493 Juergen Bader, Paolo Ruti, Fabrice Chauvin, 2011:[Changes in the interannual SST-forced](#)

1494 [signals on West African rainfall. AGCM intercomparison](#) Climate dynamics 37 (9-10),  
1495 1707-1725.  
1496  
1497 Molod, A., L. Takacs, M. Suarez, J. Bacmeister, I.-S. Song, and A. Eichmann, 2012: The  
1498 GEOS-5 Atmospheric General Circulation Model: Mean Climate and Development  
1499 from MERRA to Fortuna. NASA Tech. Rep. Series on Global Modeling and Data  
1500 Assimilation, NASA TM—2012-104606, Vol. 28, 117 pp.  
1501  
1502 Mueller, B., and S.I. Seneviratne, 2012: Hot days induced by precipitation deficits at the  
1503 global scale. Proc. Natl Acad. Sci., 109 (31), 12398-12403, doi:  
1504 [10.1073/pnas.1204330109](https://doi.org/10.1073/pnas.1204330109)  
1505  
1506 Müller, O. V., E. H. Berbery, D. Alcaraz-Segura, and M. B. Ek, 2014: Regional Model  
1507 Simulations of the 2008 Drought in Southern South America Using a Consistent Set of  
1508 Land Surface Properties. J. Climate, 27, 6754–6778.  
1509 doi: <http://dx.doi.org/10.1175/JCLI-D-13-00463.1>  
1510  
1511 NDMC (2014): ENSO and Drought Around the World.  
1512 (<http://drought.unl.edu/DroughtBasics/ENSOandForecasting.aspx>).  
1513  
1514 Parry, S., J. Hannaford, B. Lloyd-Hughes, C. Prudhomme, and C. Keef, 2010:  
1515 Drought Summaries of Spatio-temporal evolution of major European Droughts since

1516 1960. Environment Agency Science Report SC070079, Environment Agency, Bristol.  
1517

1518 Poveda, G. and O. J. Mesa, 1997: Feedbacks between Hydrological Processes in Tropical  
1519 South America and Large-Scale Ocean–Atmospheric Phenomena. *J. Climate*, 10, 2690–  
1520 2702.  
1521 doi: [http://dx.doi.org/10.1175/1520-0442\(1997\)010<2690:FBHPIT>2.0.CO;2](http://dx.doi.org/10.1175/1520-0442(1997)010<2690:FBHPIT>2.0.CO;2)  
1522

1523 Qian C., and T. Zhou, 2014: Multidecadal variability of North China aridity and its  
1524 relationship to PDO during 1900-2010, *J. Climate*, 27(3), 1210-1222.  
1525

1526 Orłowsky, B., and S.I. Seneviratne, 2012: Global changes in extreme events: Regional  
1527 and seasonal dimension. *Climatic Change*, 110, 669-696, doi: 10.1007/s10584-011-0122-  
1528 9.  
1529

1530 Orłowsky, B. and S.I. Seneviratne, 2013: Elusive drought: uncertainty in observed trends  
1531 and short- and long-term CMIP5 projections, *Hydrol. Earth Syst. Sci.*, 17, 1765-1781,  
1532 doi:10.5194/hess-17-1765-2013.  
1533

1534 Orth, R. and S.I. Seneviratne, 2014. Predictability of soil moisture and streamflow on  
1535 sub-seasonal timescales: A case study. *J. Geophysical Res. - Atmospheres*, 118: 10963-  
1536 10979.  
1537

1538 Ramanathan, V., Chung, C., Kim, D., Bettge, T., Buja, L., Kiehl, J. T., Washington, W.  
1539 M., Fu, Q., Sikka, D. R., and Wild, M., 2005: Atmospheric brown clouds: Impacts on  
1540 South Asian climate and hydrological cycle, *Proc. Natl. Acad. Sci. USA*, 102, 5326–  
1541 5333.

1542

1543 Rayner, N.A., D.E. Parker, E.B. Horton, C.K. Folland, L.V. Alexander, D.P. Rowell,  
1544 E.C. Kent, and A. Kaplan, 2003: Global analyses of sea surface temperature, sea ice, and  
1545 night marine air temperature since the late Nineteenth Century. *J. Geophys. Res.*, 108,  
1546 (D14), 4407. doi:10.1029/2002JD002670

1547

1548 Richter, I., 2015: Climate model biases in the eastern tropical oceans: causes, impacts and  
1549 ways forward. *Wiley Inter. Rev: Clim. Change*, 6, 345–358, doi:10.1002/wcc.338.

1550

1551 Rienecker, M. M., and Coauthors, 2008: The GEOS-5 data assimilation system—  
1552 Documentation of versions 5.0.1, 5.1.0, and 5.2.0. NASA Tech. Rep. Series on Global  
1553 Modeling and Data Assimilation, NASA/TM-2007-104606, Vol. 27, 95 pp.

1554

1555 Robson, J., R. Sutton, K. Lohmann, D. Smith, M. Palmer, 2012: The causes of the rapid  
1556 warming of the North Atlantic Ocean in the mid 1990s. *J. Climate*, 25, 4116-4134.

1557

1558 Rodell, M., P. R. Houser, U. Jambor, J. Gottschalck, K. Mitchell, C.-J. Meng, K.  
1559 Arsenault, B. Cosgrove, J. Radakovich, M. Bosilovich, J. K. Entin, J. P. Walker, D.  
1560 Lohmann, and D. Toll, The Global Land Data Assimilation System, *Bull. Amer. Meteor.*

1561 Soc., 85(3): 381-394, 2004.

1562

1563 Rodríguez-Fonseca, B., I. Polo, J. García-Serrano, T. Losada, E. Mohino, C. R. Mechoso,  
1564 and F. Kucharski, 2009: Are Atlantic Niños enhancing Pacific ENSO events in recent  
1565 decades? *Geophys. Res. Lett.*, 36, L20705, doi:10.1029/2009GL040048.

1566

1567 Rodríguez-Fonseca, B., S. Janicot, E. Mohino, T. Losada, J. Bader, Cyril Caminade,  
1568 Fabrice Chauvin, Bernard Fontaine, Javier García-Serrano, Sebastien Gervois, Mathieu  
1569 Joly, Irene Polo, Paolo Ruti, Pascal Roucou, Aurore Voltaire, 2011:  
1570 Interannual and decadal SST-forced responses of the West African monsoon.  
1571 *Atmospheric Science Letters*, 12(1), 67-74.

1572

1573 Rodríguez-Fonseca, B., E. Mohino, C.R. Mechoso, C. Caminade, M. Biasutti, M.  
1574 Gaetani, J. Garcia-Serrano, E.K. Vizy, K. Cook, Y. Xue, I. Polo, T. Losada, L. Druyan,  
1575 B. Fontaine, J. Bader, F.J. Doblas-Reyes, L. Goddard, S. Janicot, A. Arribas, W. Lau, A.  
1576 Colman, M. Vellinga, D.P. Rowell, F. Kucharski, and A. Voltaire, 2015: Variability and  
1577 predictability of West African droughts: A review of the role of sea surface temperature  
1578 anomalies. *J. Climate*, in press, doi:10.1175/JCLI-D-14-00130.

1579

1580 Roeckner, E., G. Bäuml, L. Bonaventura, R. Brokopf, M. Esch, M. Giorgetta, S.  
1581 Hagemann, I. Kirchner, L. Kornblueh, E. Manzini, A. Rhodin, U. Schlese, U.  
1582 Schulzweida, and A. Tompkins, 2003: The atmospheric general circulation model  
1583 ECHAM5. Part I: Model description. Max Planck Institute for Meteorology Rep. 349,



1584 127 pp. [available from MPI for Meteorology, Bundesstr. 53, 20146 Hamburg,  
1585 Germany].

1586

1587 Ropelewski, C. F., and M. S. Halpert ,1987: Global and regional scale precipitation  
1588 patterns associated with the El Niño/ Southern Oscillation. Mon. Wea. Rev., 115, 1606-  
1589 1626.

1590

1591 Rowell, D. P., 2013: Simulating SST Teleconnections to Africa: What is the State of the  
1592 Art?. J. Climate, 26, 5397–5418. doi: <http://dx.doi.org/10.1175/JCLI-D-12-00761.1>

1593

1594 [Sánchez, E. and coauthors, 2015: Regional climate modelling in CLARISLPB: a](#)  
1595 [concerted approach towards twenty-first century projections of regional temperature and](#)  
1596 [precipitation over South America, Climate Dyn. DOI 10.1007/s00382-014-2466-0.](#)

1597

1598 Saravanan R. and P. Chang, 2000: Interaction between tropical Atlantic variability and  
1599 El Niño-Southern Oscillation. J. Climate 13, 2177–2194.

1600

1601 Scaife, A.A., J.R. Knight, G.K. Vallis, C.K. Folland, 2005: A stratospheric influence on  
1602 the winter NAO and North Atlantic surface climate. Geophys. Res. Lett. 32, L18715.

1603

1604 Schubert, S.D., M. J. Suarez, P. J. Pegion, R. D. Koster, and J. T. Bacmeister , 2004: On  
1605 the Cause of the 1930s Dust Bowl, Science, **33**, 1855-1859.

1606 Schubert, S., D. Gutzler, H. Wang, A. Dai, T. Delworth, C. Deser, K. Findell, R. Fu, W.  
1607 Higgins, M. Hoerling, B. Kirtman, R. Koster, A. Kumar, D. Legler, D. Lettenmaier, B.  
1608 Lyon, V. Magana, K. Mo, S. Nigam, P. Pegion, A. Phillips, R. Pulwarty, D. Rind, A.  
1609 Ruiz-Barradas, J. Schemm, R. Seager, R. Stewart, M. Suarez, J. Syktus, M. Ting, C.  
1610 Wang, S. Weaver, N. Zeng, 2009: A USCLIVAR Project to Assess and Compare the  
1611 Responses of Global Climate Models to Drought-Related SST Forcing Patterns:  
1612 Overview and Results. *J. Climate*, 22, 5251–5272.  
1613  
1614 Schubert, S., H. Wang, R. Koster, M. Suarez, and P. Groisman, 2014: Northern Eurasian  
1615 Heat Waves and Droughts. *J. Climate*, 27, 3169-3207.  
1616  
1617 Seager, R., Y. Kushnir, C. Herweijer, N. Naik, and J. Velez, 2005: Modeling the tropical  
1618 forcing of persistent droughts and pluvials over western North America: 1856-2000. *J.*  
1619 *Climate*, 18, 4068-4091.  
1620  
1621 Seager, R., N. Naik, W. Baethgen, A. Robertson. Y. Kushnir, J. Nakamura, S. Jurburg,  
1622 2010: Tropical oceanic causes of interannual to multidecadal precipitation variability in  
1623 southeast South America over the past century. *J. Climate*, 23, 5517-5539.  
1624  
1625 Seager, R., L. Goddard, J. Nakamura, N. Henderson, D. E. Lee, 2014a: Dynamical causes  
1626 of the 2010/11 Texas-northern Mexico drought. *J. Hydrometeor.* 2013, 15, 39-68.  
1627

1628 Seager, R., H. Liu, N. Henderson, I. Simpson, C. Kelley, T. Shaw, Y. Kushnir and M.  
1629 Ting, 2014b: Causes of increasing aridification of the Mediterranean region in response  
1630 to rising greenhouse gases, *J. Climate*, 27, 4655-4676.  
1631  
1632 Seager, R., M. Hoerling, S. Schubert, H. Wang, B. Lyon, A. Kumar, J. Nakamura, and N.  
1633 Henderson, 2014c: Causes and predictability of the 2011–14 California drought,  
1634 DTF/NIDIS Assessment Report, 40 pp., doi:10.7289/V7258K7771F.  
1635  
1636 Seager, R. and M. Hoerling, 2014: Atmosphere and Ocean Origins of North American  
1637 Drought. *J. Climate*, 27, 4581-4606.  
1638  
1639 Seneviratne, S. I. and Coauthors, 2006: Soil moisture memory in AGCM simulations:  
1640 Analysis of Global Land–Atmosphere Coupling Experiment (GLACE) data. *J.*  
1641 *Hydrometeor.*, 7, 1090–1112.  
1642  
1643 Seneviratne, S.I., N. Nicholls, D. Easterling, C.M. Goodess, S. Kanae, J. Kossin, Y. Luo,  
1644 J. Marengo, K. McInnes, M. Rahimi, M. Reichstein, A. Sorteberg, C. Vera, and X.  
1645 Zhang, 2012a: Changes in climate extremes and their impacts on the natural physical  
1646 environment. In: *Managing the Risks of Extreme Events and Disasters to Advance*  
1647 *Climate Change Adaptation* [Field, C.B., V. Barros, T.F. Stocker, D. Qin, D.J. Dokken,  
1648 K.L. Ebi, M.D. Mastrandrea, K.J. Mach, G.-K. Plattner, S.K. Allen, M. Tignor, and P.M.  
1649 Midgley (eds.)]. A Special Report of Working Groups I and II of the Intergovernmental  
1650 Panel on Climate Change, pp. 109-230.

1651

1652 Seneviratne, S.I., I. Lehner, J. Gurtz, A.J. Teuling, H. Lang, U. Moser, D. Grebner, L.  
1653 Menzel, K. Schrott, T. Vitvar, and M. Zappa, 2012b: Swiss pre-alpine Rietholzbach  
1654 research catchment and lysimeter: Analysis of 32--year hydroclimatological time series  
1655 and 2003 drought. *Water Resources Research*, 48, W06526,  
1656 doi:10.1029/2011WR011749.

1657

1658 Sheffield, J., E.F. Wood, and M.L. Roderick, 2012: Little change in global drought in the  
1659 past 60 years. *Nature*, 491, 435-438, doi:10.1038/nature11575.

1660

1661 Smith, D.M., A.A. Scaife, and B. P. Kirtman, 2012: What is the current state of  
1662 knowledge with regard to seasonal to decadal forecasting? *Environ. Res. Lett.*, 7, 015602  
1663 (11pp).

1664

1665 Song F. and T. Zhou, 2014a: Interannual Variability of East Asian Summer Monsoon  
1666 Simulated by CMIP3 and CMIP5 AGCMs: Skill Dependence on Indian Ocean–Western  
1667 Pacific Anticyclone Teleconnection. *J. Climate*, 27, 1679–1697.

1668

1669 Song F., and T. Zhou, 2014b: The climatology and interannual variability of East Asian  
1670 summer monsoon in CMIP5 coupled models: Does air-sea coupling improve the  
1671 simulations? *J. Climate*, 27, 8761-8777

1672

1673 Song F., T. Zhou, and Y. Qian, 2014: Responses of East Asian summer monsoon to  
1674 natural and anthropogenic forcings in the 17 latest CMIP5 models, *Geophys. Res. Lett.*,  
1675 41, doi:10.1002/2013GL058705  
1676  
1677 Sörensson, A. A., and C. G. Menéndez, 2011: Summer soil–precipitation coupling in  
1678 South America. *Tellus A*, 63, 56–68. doi: 10.1111/j.1600-0870.2010.00468.x  
1679  
1680 Spinoni, J., G. Naumann, J. Vogt, and P. Barbosa, 2015: The biggest drought events in  
1681 Europe from 1950 to 2012. *J. Hydrology*, in press.  
1682  
1683 Stagge, J.H., I. Kohn, L.M. Tallaksen, and K. Stahl, 2015: Modeling drought impact  
1684 occurrence based on meteorological drought indices in Europe. *J. Hydrology*, 530, 37-50.  
1685  
1686 Stahl, K., 2001: Hydrological Drought – a Study across Europe. PhD Thesis, Albert-  
1687 Ludwigs-Universität Freiburg, Freiburger Schriften zur Hydrologie no. 15, also available  
1688 from: <<http://www.freidok.unifreiburg.de/volltexte/202>>.  
1689  
1690 Staudinger, M., K. Stahl, and J. Seibert, 2014: A drought index accounting for snow.  
1691 *Water Resour. Res.*, 50, 7861–7872, doi:10.1002/2013WR015143.  
1692  
1693 Sutton, R. and B. Dong, 2012: Atlantic Ocean influence on a shift in European climate in  
1694 the 1990s. *Nature Geoscience*, 5, pp. 788-792. ISSN 1752-0908 doi: 10.1038/ngeo1595.  
1695

1696 Tallaksen, L.M., J.H. Stagge, K. Stahl, L. Gudmundsson, R. Orth, S.I. Seneviratne, A.F.  
1697 van Loon, and H.A.J. van Lanen, 2015: Characteristics and drivers of drought in Europe  
1698 – a summary of the DROUGHT-RSPI project. In: “Drought: Research and Science-  
1699 Policy Interfacing”, Andreu et al. (eds). Taylor & Francis Group, London, ISBN 978-1-  
1700 138-02779-4.  
1701  
1702 Teuling, A.J., A. van Loon, S.I. Seneviratne, I. Lehner, M. Aubinet, B. Heinesch, C.  
1703 Bernhofer, T. Grünwald, H. Prasse, and U. Spank, 2013: Evapotranspiration amplifies  
1704 European summer drought. *Geophys. Res. Lett.*, 40 (10), 2071-2075  
1705  
1706 Van Loon, A. F., and H.A. Van Lanen, 2012. A process-based typology of hydrological  
1707 drought, *Hydrol. Earth Syst. Sci.*, 16: 1915–1946.  
1708  
1709 Vicente-Serrano, Sergio M., Santiago Beguería, and Juan I. López-Moreno, 2010: A  
1710 Multiscalar Drought Index Sensitive to Global Warming: The Standardized Precipitation  
1711 Evapotranspiration Index. *J. Climate*, **23**, 1696–1718.  
1712 doi: <http://dx.doi.org/10.1175/2009JCLI2909.1>  
1713  
1714 Wang, G., Y. Kim, and D. Wang, 2007: Quantifying the strength of soil moisture-  
1715 precipitation coupling and its sensitivity to changes in surface water budget. *J.*  
1716 *Hydrometeorol.*, 8, 551–570.  
1717

1718 Wang, C., S.-K. Lee, and D. B. Enfield, 2008: Climate Response to Anomalously Large  
1719 and Small Atlantic Warm Pools during the Summer. *J. Climate*, 21, 2437–2450. doi:  
1720 <http://dx.doi.org/10.1175/2007JCLI2029.1>  
1721

1722 Wang, H., S.D. Schubert, M. J. Suarez, J. Chen, M. Hoerling, A. Kumar and P. Pegion,  
1723 2009: Attribution of the seasonality and regionality in climate trends over the United  
1724 States during 1950-2000. *J. Climate*, 2571-2590.  
1725

1726 Wang, H., S. Schubert, R. Koster, Y.-G. Ham, and M. Suarez, 2014: On the Role of SST  
1727 Forcing in the 2011 and 2012 Extreme U.S. Heat and Drought: A Study in Contrasts. *J.*  
1728 *Hydrometeor*, **15**, 1255–1273.  
1729 doi: <http://dx.doi.org/10.1175/JHM-D-13-069.1>  
1730

1731 Wu B., T. Zhou, T. Li, 2009, Seasonally Evolving Dominant Interannual Variability  
1732 Modes of East Asian Climate, *J. Climate*, 22, 2992-3005  
1733

1734 Wu B., T. Li, and T. Zhou, 2010: Relative contributions of the Indian Ocean and local  
1735 SST anomalies to the maintenance of the western North Pacific anomalous anticyclone  
1736 during El Nino decaying summer. *J. Climate*, 23, 2974-2986.  
1737

1738 Wu R., Z. Hu, and B. Kirtman, 2003: Evolution of ENSO-Related Rainfall Anomalies in  
1739 East Asia. *J. Climate*, 16, 3742–3758.  
1740

1741

1742 Xie, S.-P., K. Hu, J. Hafner, H. Tokinaga, Y. Du, G. Huang, and T. Sampe, 2009: Indian  
1743 Ocean capacitor effect on Indowestern Pacific climate during the summer following El  
1744 Niño. *J. Climate*, 22, 730–747.

1745

1746 Xoplaki, E., J. F. Gonzalez-Rouco and J. Luterbacher, 2004: Wet season Mediterranean  
1747 precipitation variability: influence of large-scale dynamics and trends. *Clim. Dyn.*, 23,  
1748 63-78.

1749

1750 Xue, Y., F. de Sales, C. R. Mechoso, C. A. Nobre, H. -M. Juang, 2006: Role of Land  
1751 Surface Processes in South American Monsoon Development. *J. Climate*, 19, 741-762.

1752

1753 Yang, W., R. Seager, M.A. Cane, and B. Lyon, 2014: The East African Long Rains in  
1754 Observations and Models. *J. Climate*, 27, 7185-7202.

1755

1756 Yang, F. L., and K. M. Lau (2004), Trend and variability of China precipitation in spring  
1757 and summer: Linkage to sea-surface temperatures, *Int. J. Climatol.*, 24, 1625 – 1644,  
1758 doi:10.1002/joc.1094.

1759

1760 Yin, D., M.L. Roderick, G. Leech, F. Sun, and Y. Huang, 2014: The contribution of  
1761 reduction in evaporative cooling to higher surface air temperatures during drought.  
1762 *Geophys. Res. Lett.*, doi:10.1002/2014GL062039.

1763



1764 Yoon, J.-H., and N. Zeng, 2009: An Atlantic influence on Amazon rainfall. *Climate Dyn.*,  
1765 34, 249–264.  
1766  
1767 Zeng, N., J. D. Neelin, K.-M. Lau, and C. J. Tucker, 1999: Enhancement of interdecadal  
1768 climate variability in the Sahel by vegetation interaction. *Science*, 286, 1537-1540.  
1769  
1770 Zhang, L. and T. Zhou, 2015: Drought over East Asia: A Review, *J. Climate*, 28(8),  
1771 3375-3399.  
1772  
1773 Zhou T., R. Yu, H. Li, and B. Wang, 2008a: Ocean Forcing to Changes in Global  
1774 Monsoon Precipitation over the Recent Half-Century, *J. Climate*, 21(15), 3833–3852.  
1775  
1776 Zhou, T., L. Zhang, and H. Li, 2008b: Changes in global land monsoon area and total  
1777 rainfall accumulation over the last half century, *Geophys. Res. Lett.*,  
1778 doi:10.1029/2008GL034881.  
1779  
1780 Zhou, T., D. Gong, J. Li, and B. Li, 2009a: Detecting and understanding the multi-  
1781 decadal variability of the East Asian Summer Monsoon – Recent progress and state of  
1782 affairs. *Meteorologische Zeitschrift*, 18 (4), 455-467.  
1783  
1784 Zhou T., Wu B., B. Wang, 2009b: How well do atmospheric general circulation models  
1785 capture the leading modes of the interannual variability of the Asian-Australian  
1786 Monsoon?, *J. Climate*, 22, 1159-1173.

1787

1788 Zhou, T., Bo Wu, A. A. Scaife, S. Bronnimann, A. Cherchi, D. Fereday, A. M. Fischer, C.

1789 K. Folland, K.E. Jin, J. Kinter, J. R. Knight, F. Kucharski, S. Kusunoki, N.-C. Lau,

1790 Lijuan Li, M.J. Nath, T. Nakaegawa, A. Navarra, P. Pegion, E. Rozanov, S. Schubert, P.

1791 Sporyshev, A. Voldoire, Xinyu Wen, J. H. Yoon ,N. Zeng, 2009c: The CLIVAR C20C

1792 Project: Which components of the Asian-Australian Monsoon circulation variations are

1793 forced and reproducible? *Climate Dyn.*, 33, 1051–1068.

1794

1795 Zhou, T., F. Song, R. Lin, X. Chen and X. Chen, 2013: The 2012 North China floods:

1796 Explaining an extreme rainfall event in the context of a long-term drying tendency [in

1797 “Explaining Extreme Events of 2012 from a Climate Perspective”]. *Bull. Amer. Meteor.*

1798 *Soc.*, 94(9), S49-S51.

1799

1800 Zwiers, F. W., X. L. Wang and J. Sheng, 2000: Effects of specifying bottom boundary

1801 conditions in an ensemble of atmospheric GCM simulations. *J. Geophys. Res.*, 105, 7295-7315.

1802

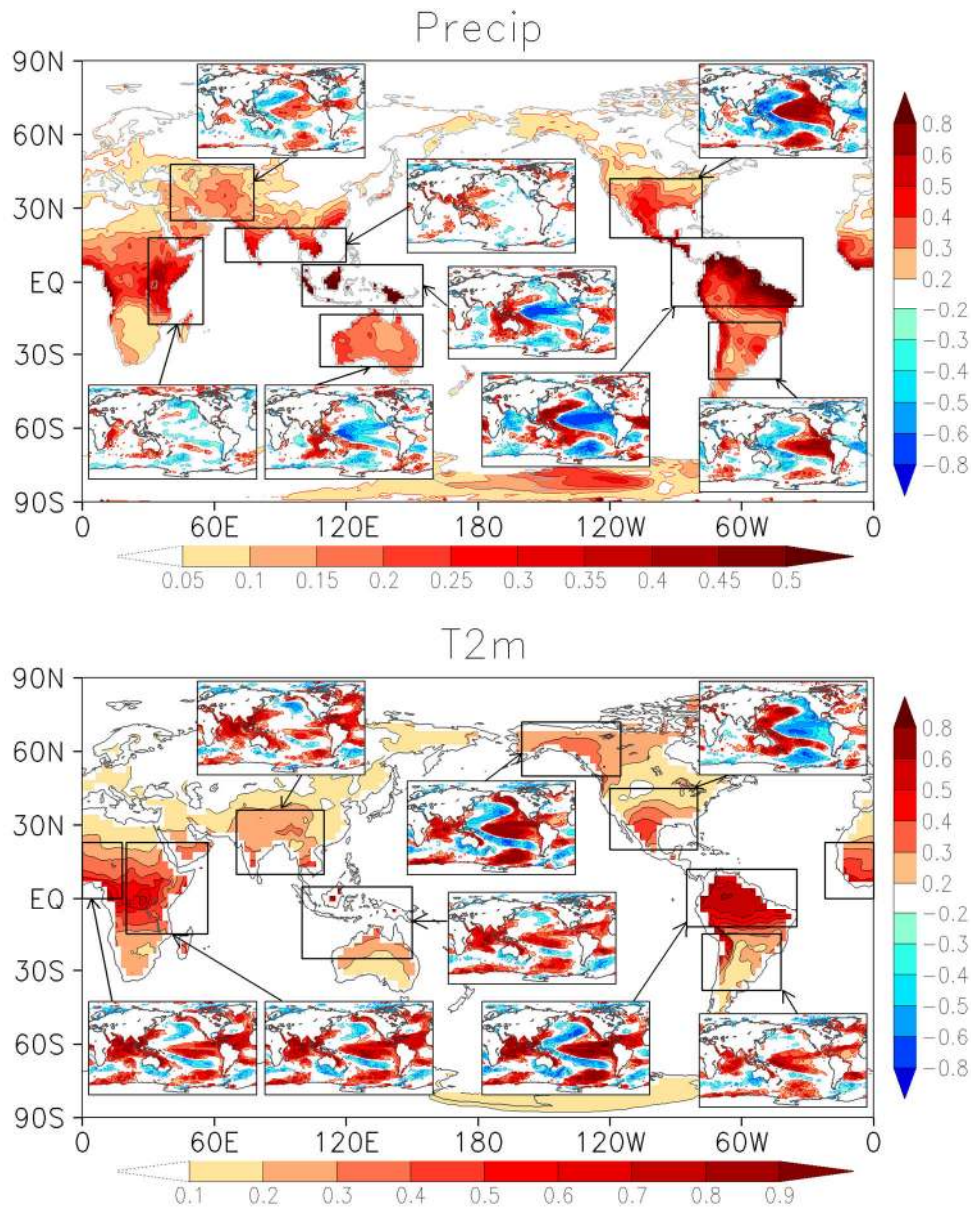
1803 *Table 1: Temporal correlation between observed annual mean regional mean*  
 1804 *precipitation (GPCP) and 1) the regional mean annual mean PDSI from Dai et al. (2004)*  
 1805 *for 1979-2005, and 2) the regional mean annual mean soil moisture (top 100cm) from the*  
 1806 *Global Land Data Assimilation System Version 2 (GLDAS-2, Rodell et al. 2004) for*  
 1807 *1979-2010. The numbers (1-10) in the Table refer to the regions outlined in Figures 5-8*  
 1808 *as follows: Figure 5: 1 (US and N. Mexico), 2 (N. South America and Central America),*  
 1809 *3 (central South America). Figure 6: 4 (west Africa), 5 (east Africa). Figure 7: 6*  
 1810 *(Mideast), 7 (southern Asia), 8 (east Asia). Figure 8: 9 (Australia), 10 (Indonesia).*

1811

|                              | 1    | 2    | 3    | 4    | 5    | 6    | 7    | 8    | 9    | 10   |
|------------------------------|------|------|------|------|------|------|------|------|------|------|
| PDSI<br>(1979-2005)          | 0.52 | 0.80 | 0.69 | 0.66 | 0.66 | 0.72 | 0.69 | 0.65 | 0.75 | 0.71 |
| Soil Moisture<br>(1979-2010) | 0.72 | 0.86 | 0.76 | 0.70 | 0.57 | 0.80 | 0.66 | 0.50 | 0.80 | 0.81 |

1812

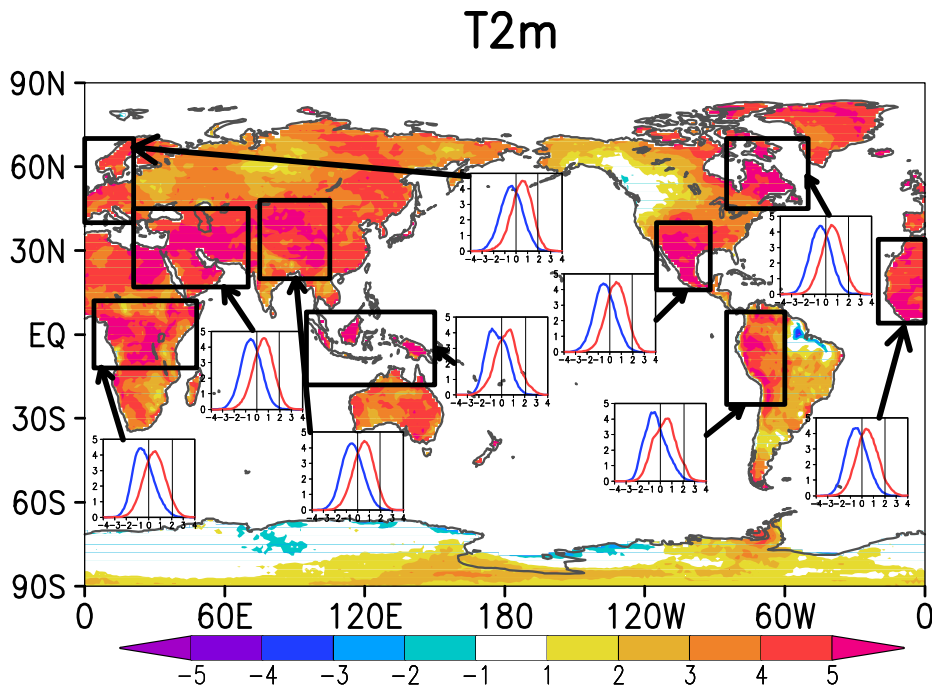
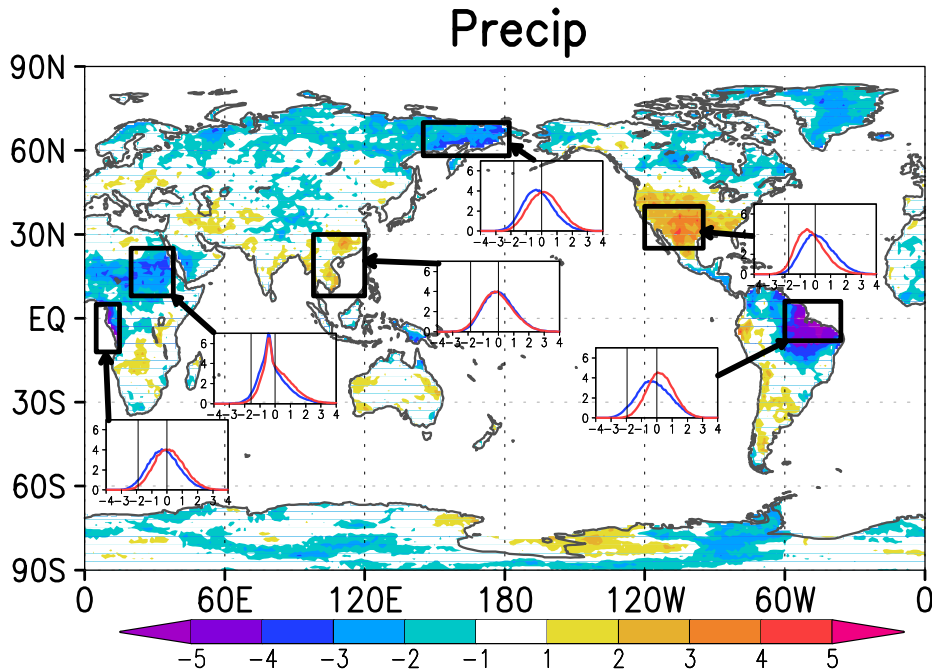
1813



1814

1815 *Figure 1. (Top) The background map shows the ratio of two variances: the variance of the*  
1816 *ensemble mean time series of annual precipitation and the total variance of annual mean*  
1817 *precipitation over all ensemble members (ratios are computed for each model separately and*  
1818 *then averaged). Higher values of the ratio indicate a stronger impact of the prescribed SSTs on*  
1819 *the precipitation time series. The small maps show the correlations between the ensemble mean*  
1820 *annual fields (averaged over the boxed areas) with SST (correlations are computed for each*  
1821 *model separately and then averaged). Results are based on 12 ensemble members for each of 5*

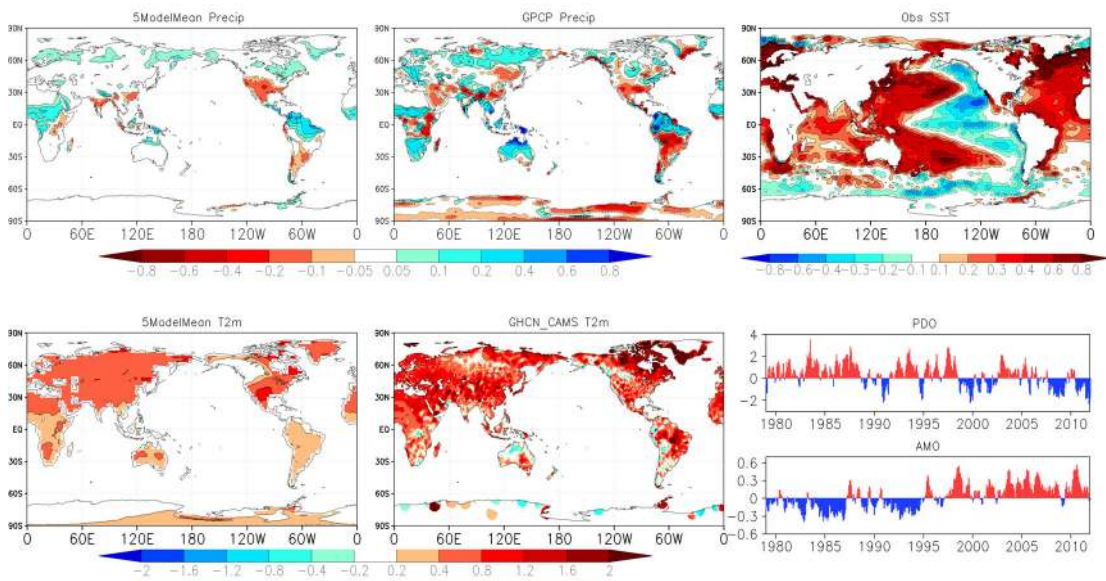
1822 *models (GEOS-5, CCM3, CAM4, GFS, ECHAM5) using detrended values for the period 1979-*  
1823 *2011. (Bottom) Same, but for 2m air temperature (note change in contour interval). The*  
1824 *horizontal color bars are for the variance ratios, and the vertical color bars are for the*  
1825 *correlations.*  
1826



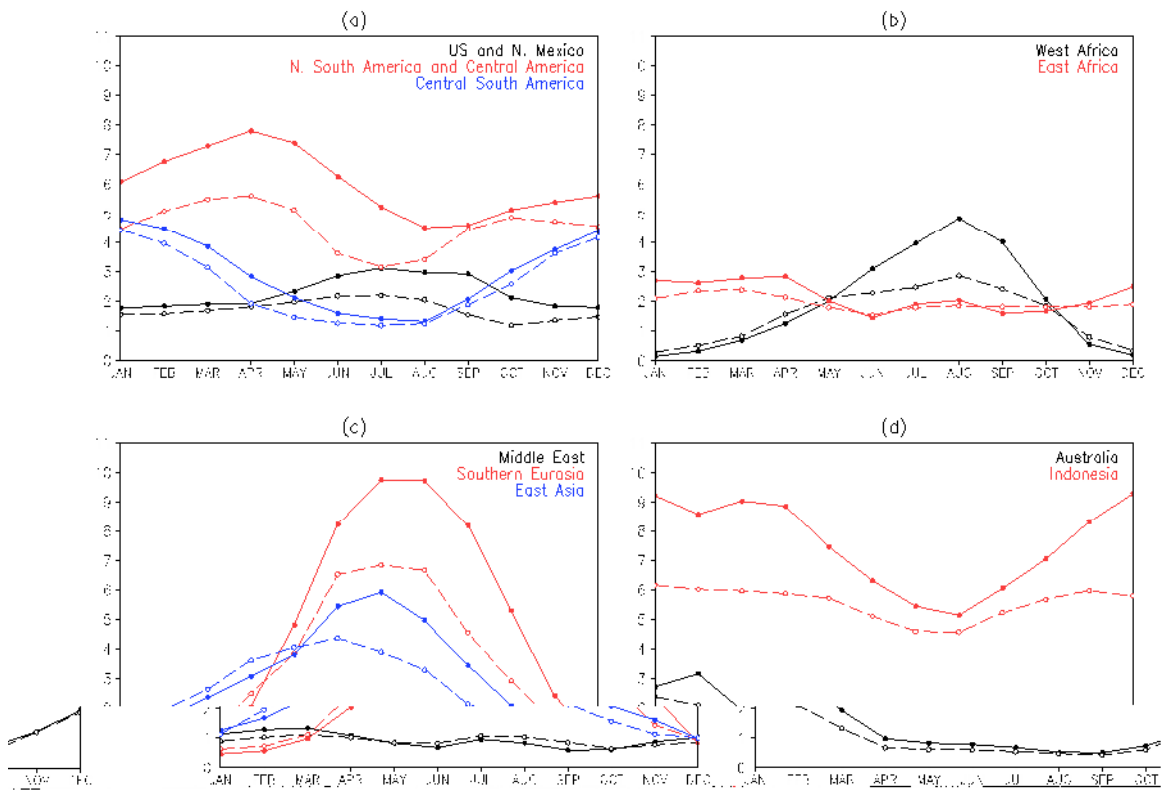
1827

1828 *Figure 2: The shift in probabilities of extremes between the two periods 1998-2011 and*  
 1829 *1979-1993 defined as  $(P(x_2 > x_c) - P(x_1 > x_c)) / P(x > x_c)$ , where  $x_2$  refers to values during the*  
 1830 *recent period (1998-2011) and  $x_1$  refers to values during the earlier period (1979-1993).*  
 1831 *The shift is normalized by  $P(x > x_c)$ , where  $x$  refers to values during the entire time period,*

1832 and  $x_c$  is chosen so that  $P(x > x_c)$  is 2.5%. The top panel shows results for precipitation  
 1833 and the bottom for 2m temperature; in the case of precipitation, the shift in probability  
 1834 actually refers to the left tail of the distribution (values less than  $x_c$ ). The results are  
 1835 based on 12 ensemble members for each of 5 models (GEOS-5, CCM3, CAM4, GFS,  
 1836 ECHAM5). Each model's values are first normalized to have zero mean and unit  
 1837 variance. The inserts show the actual PDFs for the two periods (red is for the recent  
 1838 period and blue indicates the earlier period) for all grid points in the indicated boxes,  
 1839 land only). Vertical lines highlight the zero value and the value of  $x_c$ .  
 1840



1841  
 1842 Figure 3: Top left: Mean simulated precipitation differences between 1998-2011 and 1979-1993,  
 1843 based on results from the five models. Bottom left: Corresponding differences in T2M (land  
 1844 only). Middle panels: Same as left panels, but for the observations. Top right: The mean  
 1845 observed SST differences between 1998-2011 and 1979-1993. Bottom right: the time series of the  
 1846 PDO and AMO.

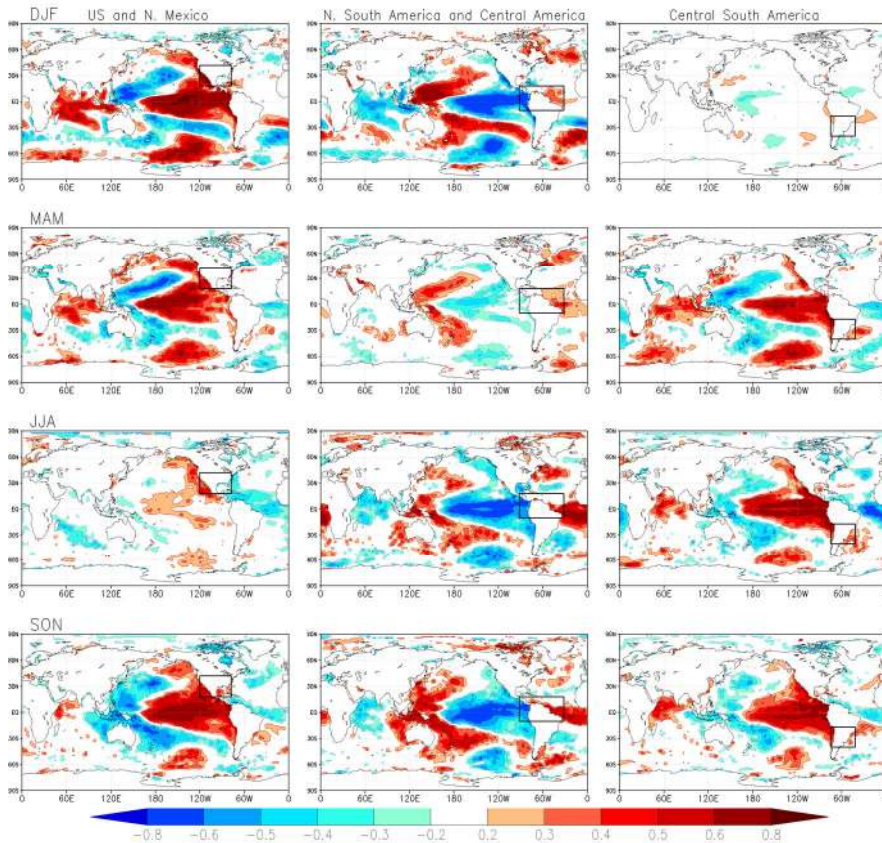


1847

1848 *Figure 4: Observed (GPCP, solid lines) and simulated (5-model ensemble mean, dashed*  
 1849 *lines) annual cycle of precipitation (mm/day) for the selected regions based on the period*  
 1850 *1979-2011. The regions (land only) are those examined in Figure 5, Figure 6, Figure 7,*  
 1851 *and Figure 8 (see the boxes outlining the regions in those figures).*

1852

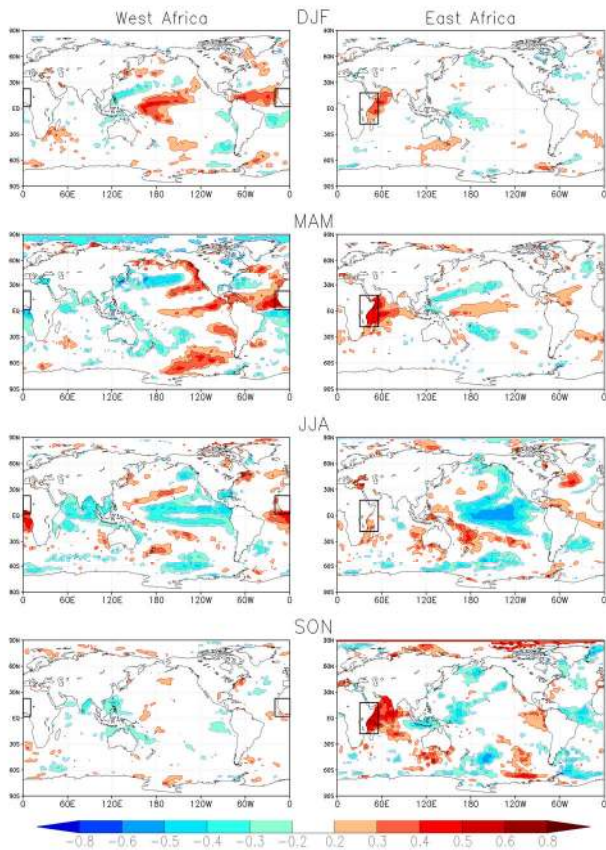




1853

1854 *Figure 5: Left panels: The correlations between the ensemble mean precipitation*  
 1855 *averaged over the United States and northern Mexico (black box) and SST for individual*  
 1856 *seasons (correlations are averaged over the 5 models). Middle panels: same as left*  
 1857 *panels, but for northern South America and Central America (black box). Right panels:*  
 1858 *Same as left panels, but for central South America (black box).*

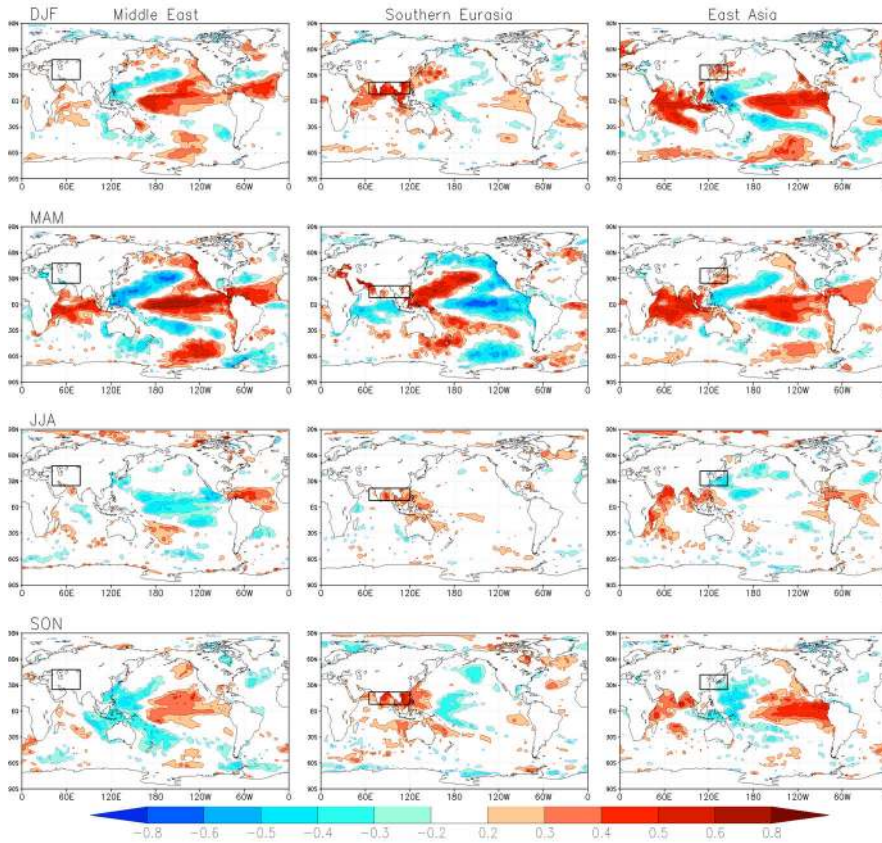
1859



1860

1861 *Figure 6: Left panels: The correlations between the ensemble mean precipitation*  
 1862 *averaged over West Africa (black box) and SST for individual seasons ((correlations are*  
 1863 *averaged over the 5 models)). Right panels: Same, but for east Africa.*

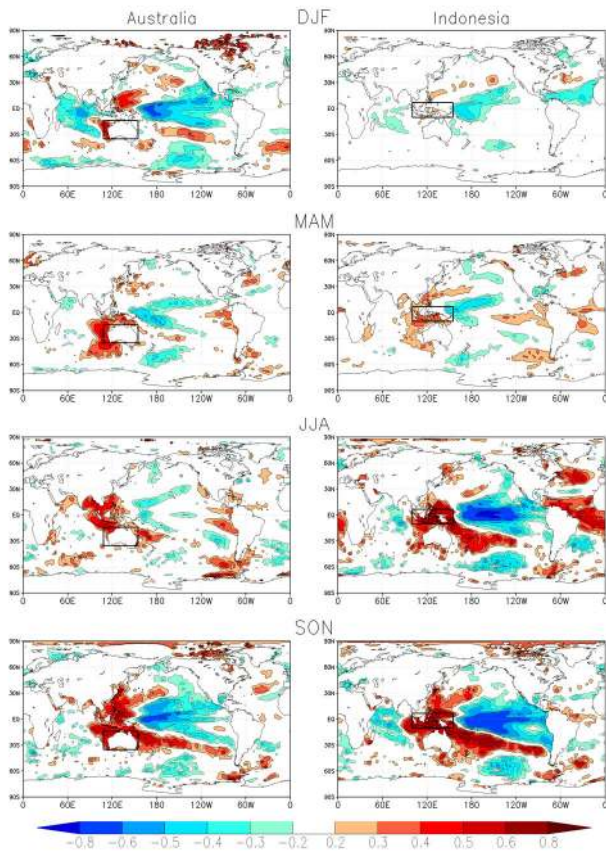
1864



1865

1866 *Figure 7: Left panels: The correlations between the ensemble mean precipitation*  
 1867 *averaged over the middle east (black box) and SST for individual seasons (correlations*  
 1868 *are averaged over the 5 models). Middle panels: Same, but for southern Eurasia. Right*  
 1869 *panels: Same, but for east Asia.*

1870



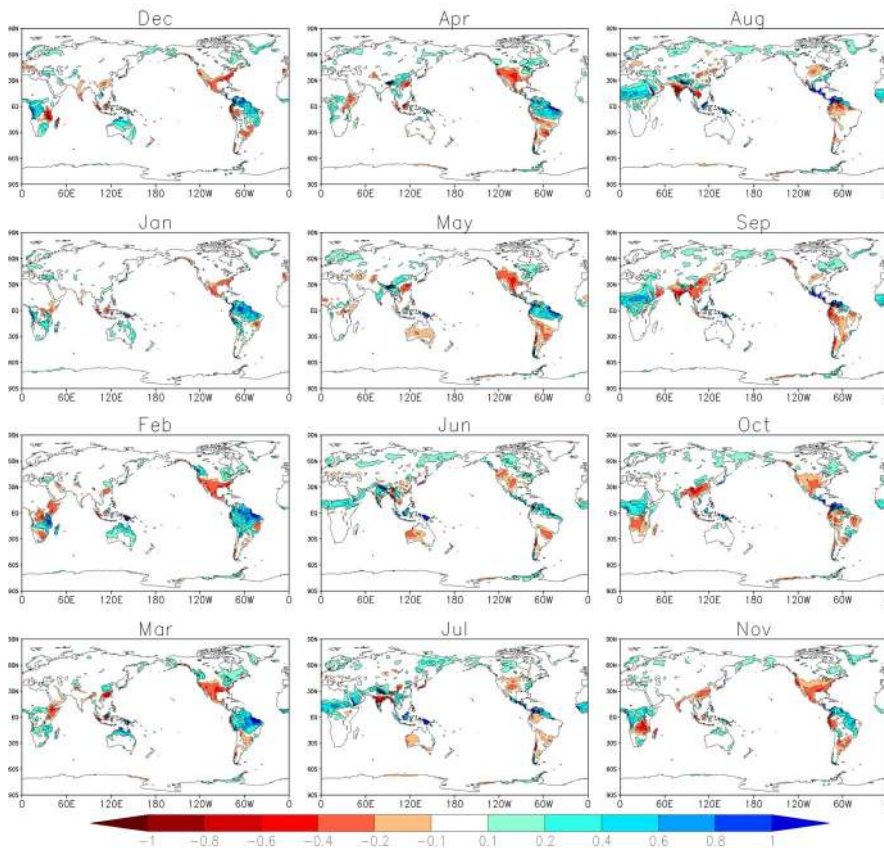
1871

1872 *Figure 8: Left panels: Correlations between the ensemble mean precipitation averaged*

1873 *over Australia (black box) and SST for individual seasons (correlations are averaged*

1874 *over the 5 models). Right panels: Same, but for Indonesia.*

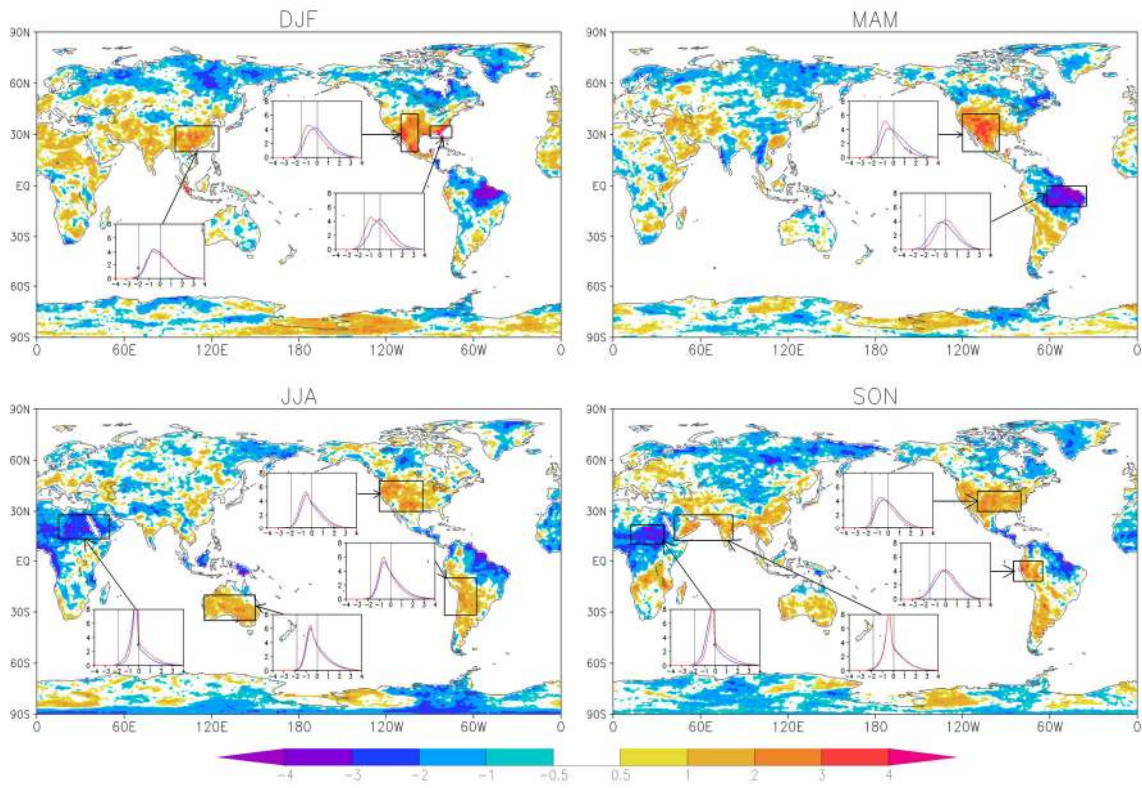
1875



1876

1877 *Figure 9: The 5-model mean simulated precipitation differences between 1998-2011 and*  
 1878 *1979-1993 for individual months. Units: mm/day.*

1879

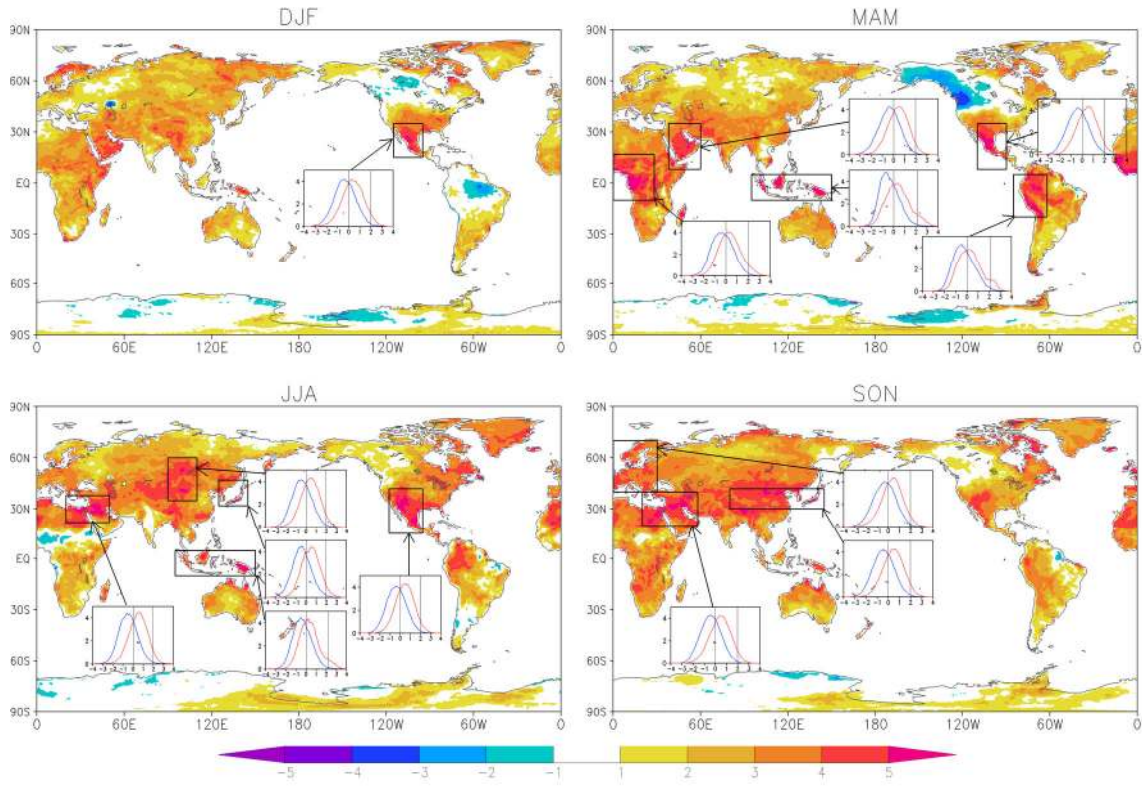


1880

1881 *Figure 10: Same as Figure 2a, but for each season.*

1882

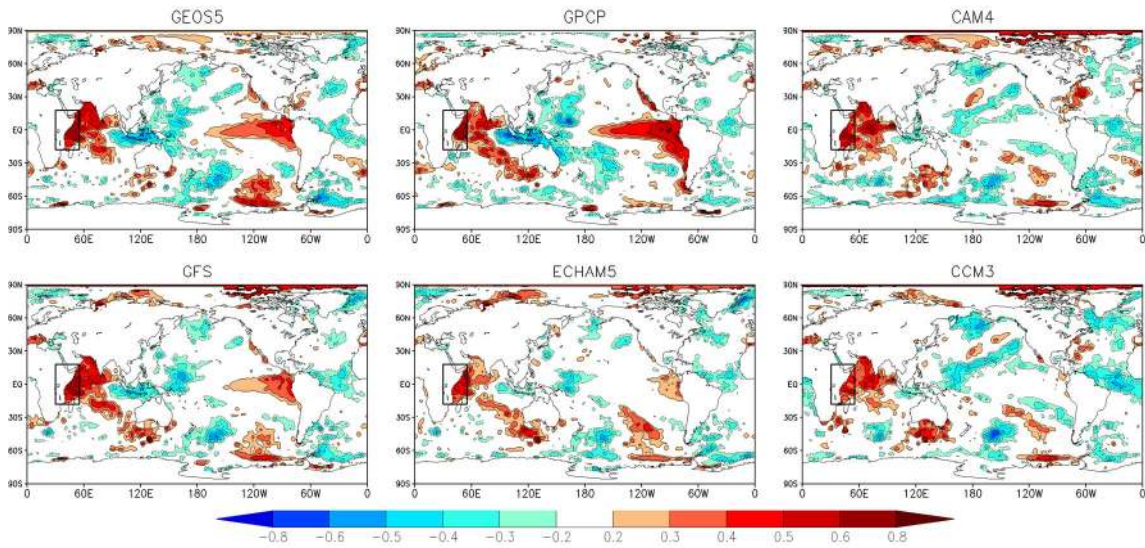
1883



1884

1885 *Figure 11: Same as Figure 2b, but for each season.*

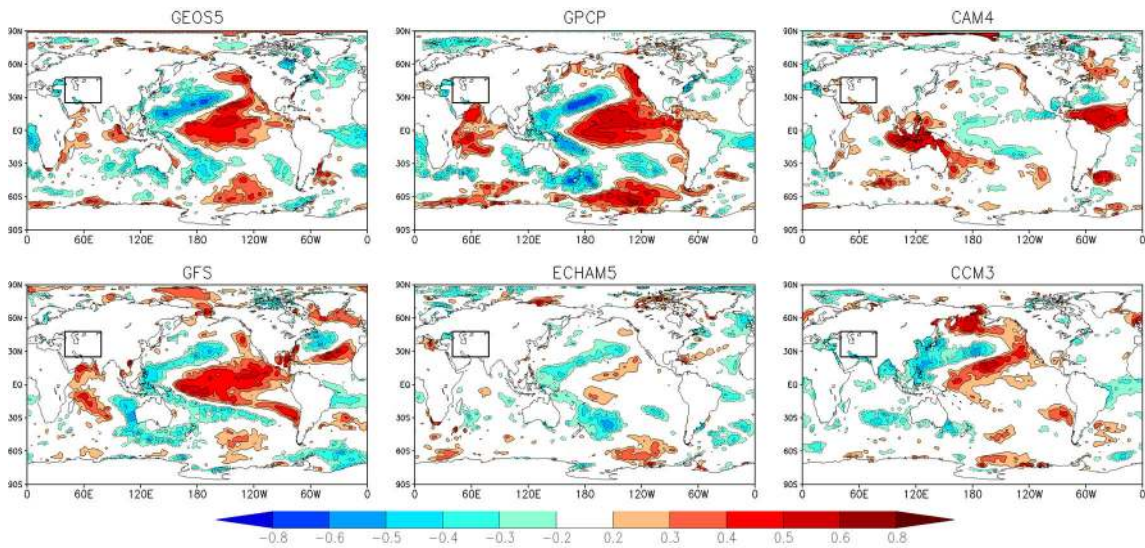
1886



1887

1888 *Figure B1: The correlations between the ensemble mean precipitation over East Africa*  
 1889 *and SST for each model during SON (1979-2011). Also shown (top middle panel) is the*  
 1890 *correlation based on GPCP observations.*

1891

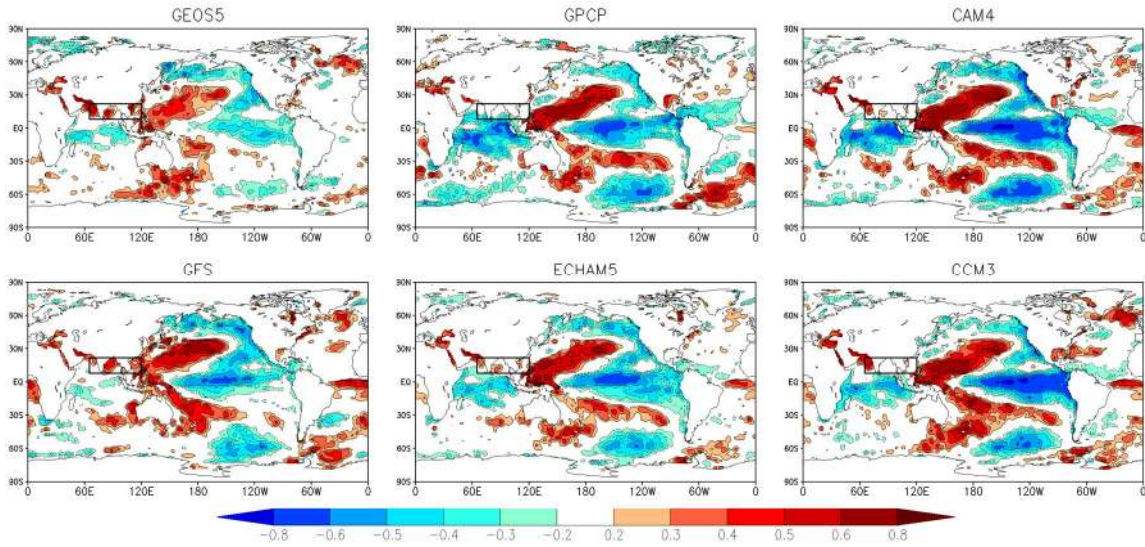


1892

1893 *Figure B2: The correlations between the ensemble mean annual precipitation over the*  
 1894 *Middle East and SST for each model (1979-2011). Also shown (top middle panel) is the*  
 1895 *correlation based on GPCP observations. We note that there is some sensitivity to the*

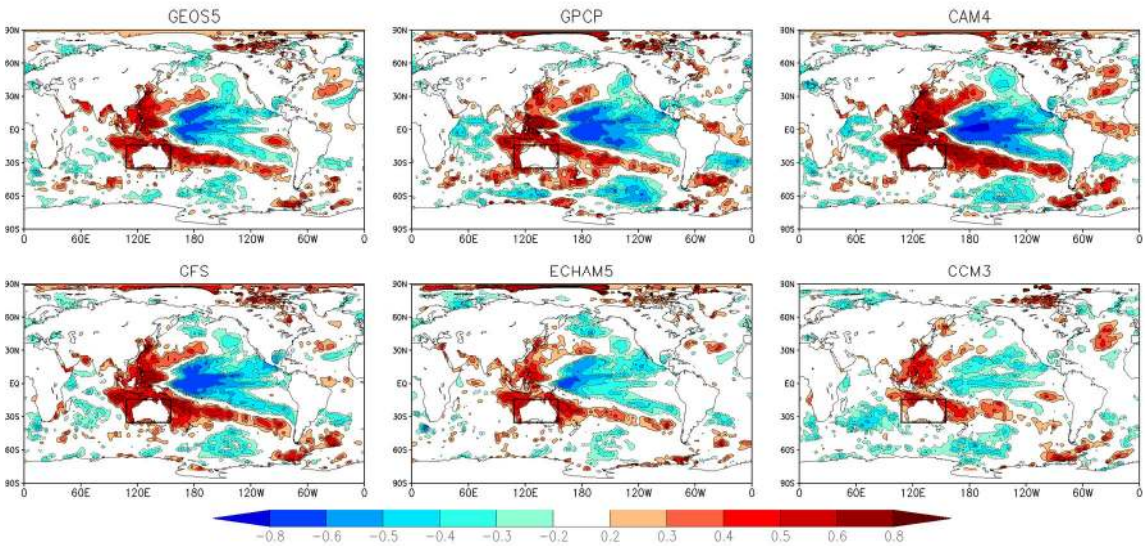


1896 region chosen for some of the models (e.g. the results for CCM3 looks more like that of  
 1897 the other models and observations if the region is truncated on the southern and eastern  
 1898 edges).



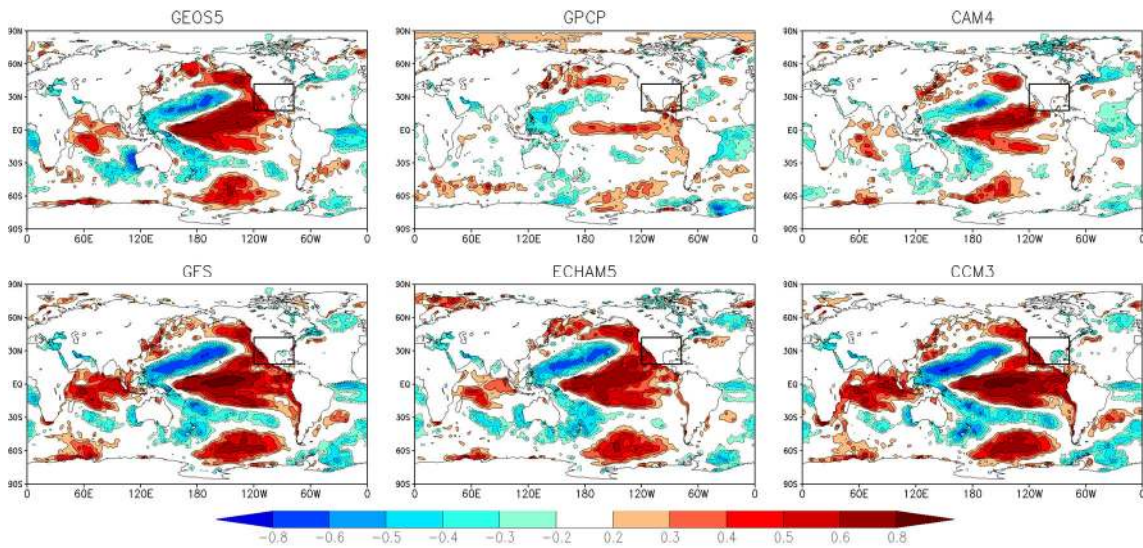
1899  
 1900 *Figure B3: The correlations between the ensemble mean precipitation over southern Asia*  
 1901 *and SST for each model for MAM (1979-2011). Also shown (top middle panel) is the*  
 1902 *correlation based on GPCP observations.*

1903



1904

1905 *Figure B4: The correlations between the ensemble mean precipitation over Australia and*  
1906 *SST for each model for SON (1979-2011). Also shown (top middle panel) is the*  
1907 *correlation based on GPCP observations.*



1908  
1909 *Figure B5: The correlations between the ensemble mean precipitation over the southern*  
1910 *US and SST for each model for MAM (1979-2011). Also shown (top middle panel) is the*  
1911 *correlation based on GPCP observations.*

1912

1913 **List of Figures**

1914 Figure 1. (Top) The background map shows the ratio of two variances: the variance of  
1915 the ensemble mean time series of annual precipitation and the total variance of annual  
1916 mean precipitation over all ensemble members. Higher values of the ratio indicate a  
1917 stronger impact of the prescribed SSTs on the precipitation time series. The small maps  
1918 show the correlations between the ensemble mean annual fields (averaged over the boxed  
1919 areas) with SST. All results are for the period 1979-2011 and are based on 60 ensemble  
1920 members: 12 AMIP simulations for each of 5 models (GEOS-5, CCM3, CAM4, GFS,  
1921 ECHAM5). Results are based on detrended values. (Bottom) Same, but for 2m air  
1922 temperature (note change in contour interval). The horizontal color bars are for the  
1923 variance ratios, and the vertical color bars are for the correlations.

1924

1925 Figure 2: The shift in probabilities of extremes between the two periods 1998-2011 and  
1926 1979-1993 defined as  $(P(x_2 > x_c) - P(x_1 > x_c)) / P(x > x_c)$ , where  $x_2$  refers to values during the  
1927 recent period (1998-2011) and  $x_1$  refers to values during the earlier period (1979-1993).  
1928 The shift is normalized by  $P(x > x_c)$ , where  $x$  refers to values during the entire time period,  
1929 and  $x_c$  is chosen so that  $P(x > x_c)$  is 2.5%. The top panel shows results for precipitation  
1930 and the bottom for 2m temperature; in the case of precipitation, the shift in probability  
1931 actually refers to the left tail of the distribution (values less than  $x_c$ ). The results are based  
1932 on 12 ensemble members for each of 5 models (GEOS-5, CCM3, CAM4, GFS,  
1933 ECHAM5). Each model's values are first normalized to have zero mean and unit  
1934 variance. The inserts show the actual PDFs for the two periods (red is for the recent

1935 period and blue indicates the earlier period) for all grid points in the indicated boxes, land  
1936 only). Vertical lines highlight the zero value and the value of  $x_c$ .

1937 Figure 3: Top left: Mean simulated precipitation differences between 1998-2011 and  
1938 1979-1993, based on results from the five models. Bottom left: Corresponding  
1939 differences in T2M (land only). Middle panels: Same as left panels, but for the  
1940 observations. Top right: The mean observed SST differences between 1998-2011 and  
1941 1979-1993. Bottom right: the time series of the PDO and AMO.

1942 Figure 4: Observed (GPCP, solid lines) and simulated (5-model ensemble mean, dashed  
1943 lines) annual cycle of precipitation (mm/day) for the selected regions based on the period  
1944 1979-2011. The regions are those examined in Figure 5, Figure 6, Figure 7, and Figure 8  
1945 (see the boxes outlining the regions in those figures).

1946 Figure 5: Left panels: The correlations between the ensemble mean precipitation  
1947 averaged over the United States and northern Mexico (black box) and SST for individual  
1948 seasons (correlations are averaged over the 5 models). Middle panels: same as left  
1949 panels, but for northern South America and Central America (black box). Right panels:  
1950 Same as left panels, but for central South America (black box).

1951

1952

1953 Figure 6: Left panels: The correlations between the ensemble mean precipitation  
1954 averaged over the Sahel (black box) and SST for individual seasons (5-model mean).

1955 Right panels: Same, but for east Africa.

1956

1957 Figure 7: Left panels: The correlations between the ensemble mean precipitation  
1958 averaged over the middle east (black box) and SST for individual seasons (5-model  
1959 mean). Middle panels: Same, but for southern Eurasia. Right panels: Same, but for east  
1960 Asia.

1961

1962 Figure 8: Left panels: Correlations between the ensemble mean precipitation averaged  
1963 over Australia (black box) and SST for individual seasons (5-model mean). Right panels:  
1964 Same, but for Indonesia.

1965

1966 Figure 9: The 5-model mean simulated precipitation differences between 1998-2011 and  
1967 1979-1993 for individual months. Units: mm/day.

1968

1969 Figure 10: Same as Figure 2a, but for each season.

1970

1971 Figure 11: Same as Figure 2b, but for each season.

1972

1973

1974 Figure B1: The correlations between the ensemble mean precipitation over East Africa  
1975 and SST for each model during SON (1979-2011). Also shown (top middle panel) is the  
1976 correlation based on GPCP observations.

1977

1978 Figure B2: The correlations between the ensemble mean annual precipitation over the  
1979 Middle East and SST for each model (1979-2011). Also shown (top middle panel) is the

1980 correlation based on GPCP observations. We note that there is some sensitivity to the  
1981 region chosen for some of the models (e.g. the results for CCM3 looks more like that of  
1982 the other models and observations if the region is truncated on the southern and eastern  
1983 edges).

1984

1985 Figure B3: The correlations between the ensemble mean precipitation over southern Asia  
1986 and SST for each model for MAM (1979-2011). Also shown (top middle panel) is the  
1987 correlation based on GPCP observations.

1988

1989 Figure B4: The correlations between the ensemble mean precipitation over Australia and  
1990 SST for each model for SON (1979-2011). Also shown (top middle panel) is the  
1991 correlation based on GPCP observations.

1992

1993 Figure B5: The correlations between the ensemble mean precipitation over the southern  
1994 US and SST for each model for MAM (1979-2011). Also shown (top middle panel) is  
1995 the correlation based on GPCP observations.